Projecto MOBIDYCS – POCTI/BSE/33735/00

RELATÓRIO FINAL

FINAL REPORT

EXECUÇÃO MATERIAL

MOBIDYCS

Integração dos processos de bioturbação e biodeposição em modelos hidrodinâmicos e de transporte de sedimentos contaminados

Integrating bioturbation and biodeposition processes in hydrodynamic and transport models for contaminated sediments

IMAR FCTUNL MARETEC – IST

Março 2004

TABLE OF CONTENTS

SUMMARY

In this final report the main achievements of the MOBIDYCS project that was developed from October 2001- October 2004 are summarized.

Several methodological improvements are considered in order to optimize future experiments.

The main results from laboratory experiments and modelling are pointed out, and gaps that should be filled in future research are emphasized.

The bioturbating species chosen was *Nereis diversicolor*, the ragworm, a common species in Portuguese estuaries and easy to get fresh from bait collectors.

Sediment was obtain in Ponta da Erva (Tagus estuary) and contaminated with copper (directly manipulating the sediment or through the overlying water).

Biogeochemical properties of the sediment were measured (surface and depth profiles) before erosion.

Erosion runs were performed using annular flumes following a stepwise increase in current velocity. During erosion runs, water samples were taken to quantify inputs from the sediment.

ADV measurements were made to characterize the hydrodynamics in the flume at several current velocities and were used to validate the results of a numerical model.

In this project we have been able to quantify the effects of bioturbation, contamination and both combined effects on the erosion of cohesive sediments and the consequent input of materials to the water column. These materials were suspended particulate matter (SPM), copper (particulate and dissolved), chlorophyll a, pheopigments, and carbohydrates (as saline and EDTA extractable extra cellular polymeric substances, EPS).

We found that bioturbation increases the inputs of SPM and chlorophyll *a* to the water column and that under contamination the effects are higher and include increased inputs of pheopigments and EPS. Contamination effects are variable and difficult to interpret since contamination affects activity but at the same times increases chlorophyll

degradation and EPS production. Mortality caused by copper toxicity and organic matter degradation further complicates the effects of bioturbation and contamination. SPM, pheopigments and EPS-EDTA are greatly increased by copper contamination. Combined effects of bioturbation and copper contamination increased SPM from 2-4 times and pheopigments 6 times.

Biological activity greatly influences/modifies sediment properties and must be taken into account for the sake of realistic modelling approaches to sediment transport in low energy systems.

A numerical estuarine, coastal and ocean hydrodynamic and transport model was adapted and developed in order to simulate a small scale system such as an annular flume. This adaptation constitutes an advance in sediment transport modelling, as it allowed e controlled laboratory experiments and to tune modelling parameterizations and validate modelling approaches, which will ultimately improve realistic sediment transport model applications to estuarine systems.

1. Introduction

1.1. Overview

The erosion of natural sediments is dependent on water currents, on sediment granulometry and mud cohesiveness and on the activities of the biota that modify the physical and chemical properties of the sediment. Bioturbating activities (sediment mixing by tube dwellers, surface disturbance by deposit feeders) are known to modify sediment geochemistry and enhance the transfer of contaminants from the water column to the sediment as well as their distribution within the sediment.
Erosion resistance and resuspension threshold of estuarine fine sediment is therefore complex and it is now accepted that it cannot be readily predicted from physical proprieties alone. However biological activity has not yet been combined satisfactorily with physical properties of sediments in models predicting sediment mobility and transport. This project was directed to generate new inputs to these models.

Therefore our **main objective** was to investigate the influence of bioturbation on erosion, resuspension and transport of contaminated and non-contaminated cohesive sediments, using an infaunal species and a wide range of current velocities. We examined:

- The modification of sediment properties and erodibility by bioturbation activities
- The modification of sediment properties and erodibilty of sediments exposed to contamination
- Combined effects of bioturbation and contamination on sediment erosion
- The effects of bioturbation in the transfer of contaminants and other materials (suspended particles, pigments and carbohydrates) from the sediment to the water column

1.2. Innovation

Innovation in the framework of this project:

- Use of stainless steel boxes shaped as flume sections for collection of undisturbed samples of sediment, that reproduce field conditions;
- Use of "ring corers" allowing easy separation of 1cm sediment layers and improving speed of analysis;
- Examination of combined bioturbation and contamination effects on erosion and erosion thresholds;
- ADV current velocity profiles performed in the annular channel, used to compare and calibrate modelling results;
- Hydrodynamic model applications at the annular channel scale using two different models: MOHID Water Modelling System, developed at Instituto Superior Técnico and improved in the framework of this project, and FLUENT, a commercial computational fluid dynamics modelling package, used at a comparative level, due to its greater affinity to simulate small scale processes. Both model results were compared with measured ADV data;
- Improvements were made in MOHID Water Modelling System regarding general model restructuring, to account for a better description of the environmental compartments to be modelled: atmosphere, water and sediments; adaptation of the model to simulate annular flumes, namely the inclusion of a new horizontal circular coordinate, the inclusion of a centrifugal acceleration in the inertial forces term when computing the hydrodynamic solution, the improvement of the numerical approach to compute cyclic boundary conditions; and last but not least, the addition of a sediment properties module able to compute differential erosion and improve parameterization of biological activity in the model's sediment compartment, therefore completing an important step towards an integrated modelling tool that is able to couple the combined effects of water currents, sediment erosion and deposition processes and the influence of biological activity in the sediments.

- Sediment transport modelling applications at the flume scale, reproducing laboratory experiments, improving parameterization, calibration and validation of the newly included sediment transport processes, so that future realistic estuarine scale modelling applications can be performed, merging physical and biogeochemical processes in order to better describe and understand these complex systems.

2. Material and Methods

2.1. Laboratory experiments

2.1.1. Annular Flumes and ADV current meter

Two flumes with a 10cm channel were built under this project (Fig. 1), of which one would have the ADV device permanently mounted. In this way we could at the same time perform erosion runs and measure near-bed velocities.

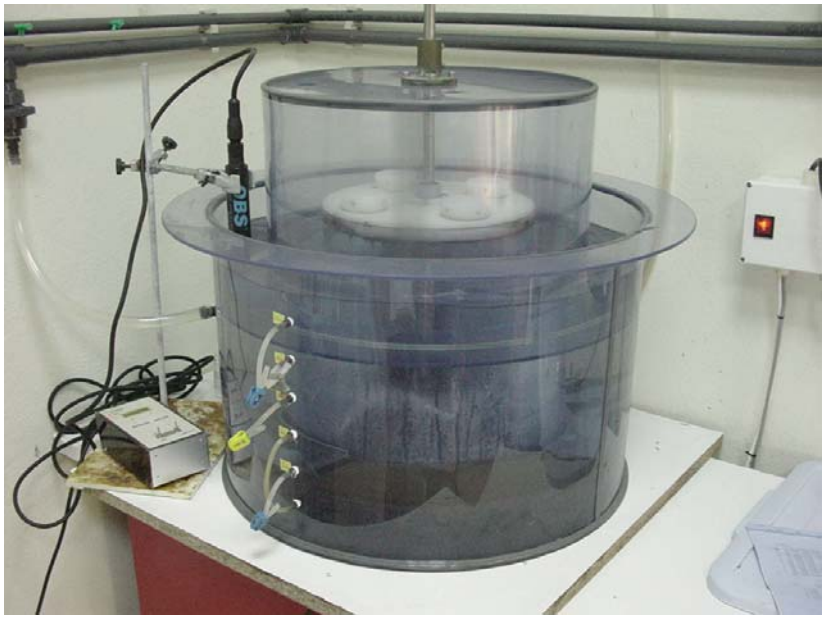

Figure 1 – Annular flume

Due to several delays in the flume construction the first experiments were performed in an existing annular flume with a 15cm channel.
Further delays occurred later on due to optimisation of the ADV mount (moving device up and down along a vertical axis) and the flumes themselves (reducing secondary flows), so that it was not possible to perform erosion runs and ADV measurements simultaneously as we intended. ADV measurements in the 10cm flume were taken over a smooth bottom without sediment (Fig.2).

Figure 2 – Current meter head looking down the annular flume channel.

2.1.2. Preliminary experiments and setup

Several experiments were carried out. Preliminary experiments were made to evaluate which species to use as bioturbator, animal density, copper content of the sediments after contamination, exposure period and mortality.
After that, two main experiments were performed: one involving manipulated sediments (exp 1), the other using undisturbed sediments (exp 2). In the case of the manipulated sediments copper was added to the sediment. In the case of the undisturbed sediments copper contamination was water-borne.

Several methodological improvements were made in exp 2 as a result of some of the difficulties detected in exp 1.

It is important that no discontinuities of the bottom are present as scouring near the edges may occur, greatly increasing suspended matter, and favouring localized erosion thereafter.
As so, instead of using a work section of ¼ of the flume perfectly levelled with the surface as as in exp 1, in exp 2 we used the whole flume bottom filled with sediment.

Sediment stability is to some extent governed by extracellular polymeric substances, EPS secreted by the biota and especially by diatoms, which inhabit the first sediment layers.
Profiles of EPS and chlorophyll a in the sediment were measured in exp 2.
Several experimental details and techniques used for determination of several parameters were given in former reports and will be kept to a minimum here.

2.1.3. Selected species

Nereis diversicolor was the bioturbator selected, as it burrows in the sediment down to 15-20 cm and feeds on its surface, greatly modifying sediment properties not only at the surface (e.g. ingesting particles) but also in the deeper layers, (e.g. cementing galleries with mucus, promoting irrigation). A bivalve species (*Cerastoderma edule*) was also included in preliminary experiments but then discarded.
Nereis diversicolor were always obtained fresh from a bait collector in the Tagus estuary. Population size ranged from 10 to 15 cm (first setiger L_3= 2.24 μm ± 0.36, n=22) and dry weight 0.075 ± 0.003 ind^{-1}. Experimental density was 900 ind m^{-2},

2.1.4. Sediment

All the sediment for the experiments was collected in Ponta da Erva, in the upper Tagus estuary. Though it was not considered contaminated regarding the content of copper (31.3±3.1 μgg-1 dry weight sediment), the heavy metal used in the experiments, this sediment is cohesive and the site easily available.

In the experiment envolving manipulated sediments (exp 1), sediment was scooped from the top 2 cm In the experiment with undisturbed sediments (exp 2), sediment was collected up to 8cm deep using 1/4 section flume boxes with removable bottom. (Fig. 3) Table 1 summarizes sediment characteristics.

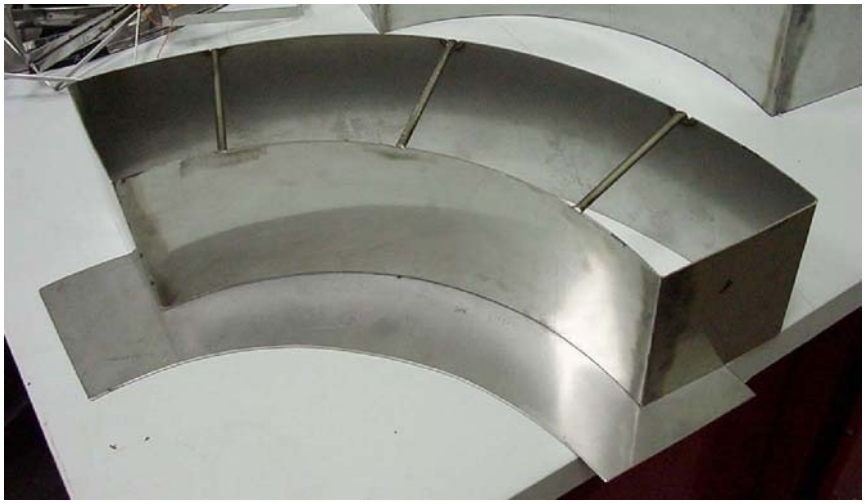

Figure 3 - Flume box for collection of undisturbed sediments.

Table 1 – Characteristics of the sediment from Ponta da Erva (upper Tagus Estuary).

	Manipulated	Non manipulated
Bulk density (Kgm-3)	1231	1295
Wet content (%)	66.1 ± 6.3	59.7 ± 2.9
Organic matter (%)	7.7 ± 1.	8.8 ± 0.6
Fine fraction (%)	95	89

2.1.5. Contamination

Sediment heavily contaminated with copper was not available and so we added copper to the collected sediment. In the case of the manipulated sediments copper was added to the sediment as copper chloride and thoroughly mixed, nominal copper content was 200 µgg-1 (dw sed). In the case of the undisturbed sediments copper contamination was water-borne, 30 µg Cu l-1.

Manipulated sediments were allowed 21d under laboratory conditions (Table 2) to stabilize and regain structure. Undisturbed sediments we left under laboratory conditions for 7d. In both, N. diversicolor was added in day 1, therefore exposure to copper was 21d in EXP1 and 7d in EXP2.

Table 2 – Laboratory conditions

Salinity	36 psu
Temperature	18± 1 ºC
Light	51 µeinstein m^{-2} s^{-1}
Photoperiod	12 h

2.1.6. Experimental design

The experimental design was the same for exp 1 and exp 2 and included four **treatments**: (1) a control treatment, **Ct** (natural sediment without macrofauna); (2) a control for *N. diversicolor* bioturbation activity, **CtNe** (natural sediment with added *N.diversicolor*; (3) a contaminated control, **CtCu** (contaminated sediment without macrofauna); and (4) a contaminated treatment with bioturbation, **CuNe** (contaminated sediment with added N.diversicolor). For all treatments one replicate flume box was kept outside the flume in the same experimental conditions for characterization of the sediment properties before erosion.

2.1.7. Erosion runs

Erosion runs were performed in two annular flumes (Table 3), following a stepwise increase in current velocity. Once the ADV measurements were not available at the time of the experiments, water velocities were calculated from previous established relationships between rpm and free-stream velocity in the flume, in close collaboration with Plymouth Marine Laboratory where the same size flume had already been calibrated.

Later, using the flume model (MARETEC team), near-bed velocities and bed-shear stress at the selected free-stream velocities were calculated.

Table 3 – Characteristics of the annular flumes

External diameter	60 cm
Channel width	15cm (EXP1); 10 cm (EXP2)
Height of the water column	30 cm
Sampling ports	7 (5 cm apart)
Current velocity range	<2 to 58 cms^{-1}

Selected velocities were chosen in such a way that we would have at least 2 to 3 velocities before and after erosion. Each increment in velocity was followed by a 20 minute period at the end of which water samples were taken to analyse several parameters. In EXP1 suspended particulate matter (SPM), dissolved organic carbon (DOC), dissolved and particulate copper (dCu, pCu), were measured and in the EXP2 chlorophyll a and carbohydrates (CHO; EPS-S and EPS-EDTA) concentration were added. As it was not possible to measure carbon in the sediment, this parameter was not considered in EXP2. (summary of measured parameters in Table 4)

In the first experiment selected velocities were <2, 5, 10, 15, 20, 25, 37 cms^{-1} and in the second experiment <2, 10, 20, 30, 40 cms^{-1}.

2.1.8. Sediment characteristics before erosion

Sediment properties measured were shear strength (fall-cone device), organic matter (incineration at 450°C for 4h), and copper content (aqua regia + HF digestion, AAS). Profiles were obtained from measurements taken in special cores (Fig. 4), at the surface (0-5mm) and then every cm (5-15mm, 15-25mm, 25-35mm, 35-45mm, 45-55mm) and >55mm.

As sediment stability is to some extent governed by extracellular polymeric substances, (EPS), mainly carbohydrates secreted by the biota and especially by diatoms, which inhabit the first sediment layers, profiles of EPS (Dubois modified method) and chlorophyll a in the sediment were measured in exp 2.

Figure 4 – Ring-corer.

2.1.9. Copper analysis

Copper concentrations in the water (APDC+DDDC extraction) were examined. Copper content (acid digestion, AAS) was also measured in the organisms (accumulation) and in the sediment.

Certified reference materials (estuarine water BCR CRM 505, mussel tissue BCR CRM 278R and marine sediment NRC MESS-3) were used to evaluate the technique used. Our values were within the confidence interval of the certified values for copper in water and sediment and were 20% lower for organisms. This was probably due to inefficient digestion of the samples.

Table 4 – Parameters measured in the experiments.

	Manipulated sediment	**Undisturbed sediment**
Water column (at selected velocities after a 20min period)	SPM (gravimetric) DOC dCu, pCu	SPM (OBS) CHO (EPS-S;EPS-EDTA) Chla dCu, pCu
Sediment (0-5mm and then every cm from up to 55 mm)	Shear strength (fall-cone), Organic matter Cu	Shear strength (fall-cone) Organic matter EPS Chla Cu
Organisms (at the start and in the end of the exposure period)	Cu	Cu

2.2. Model description

MOHID is a modular finite volumes water modelling system written in ANSI FORTRAN 95 using an object oriented programming philosophy (Braunschweig, 2004). It is an integrated modelling tool able to simulate physical and biogeochemical processes in the water column and in the sediments, and the coupling between these two domains and atmospheric processes.

The model has recently been restructured to improve the overall description, in terms of modelling, of environmental compartments: atmosphere, water and land/sediments (Fig.5). This restructuring task, induced by the objectives designed in the framework of this project, where different scientific areas meet and different approaches to study estuarine systems are made, was based on the assumption that a clear description of the system needed to be implemented, so that the inclusion and coupling of physical and biogeochemical processes occurring in the water column and in the sediment compartment would be a relatively straightforward task. This lead to a following model design: one model consisting of two main interfaces: the water-sediment interface and the water-air interface, dividing three well defined compartments, the atmosphere, the water column and the sediment. The two interfaces should be able to communicate by handling the fluxes between the three compartments. To do this, two modules were created: module *InterfaceSedimentWater* and module *InterfaceWaterAir*. Thus, for example, the water-air interface module was now responsible by processes occurring there, such as computing wind shear stress, radiation balances, latent and sensible heat fluxes and communicating with the water column (responsible for water temperature, turbidity, etc) and the atmospheric module (responsible by processes occurring in the atmosphere like wind velocity, radiation, cloud cover or precipitation, although not explicitly calculated, rather serving as a database of meteorological and atmospheric modules).

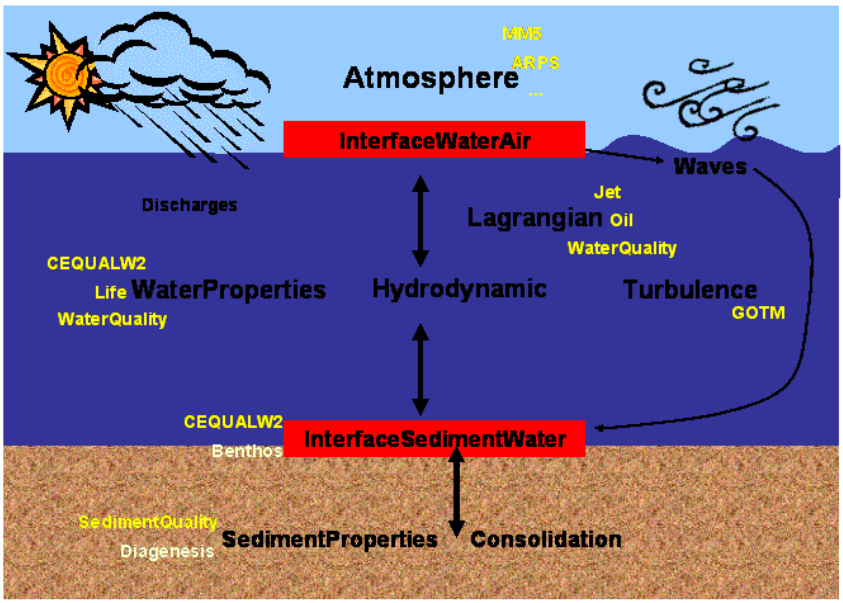

Figure 5 - MOHID modular structure

This model design enabled it to couple an integrated contaminant transport model, where contaminants can be present both in the water column and the sediment column, in the dissolved phase or adsorbed onto sediments (Fig. 6).

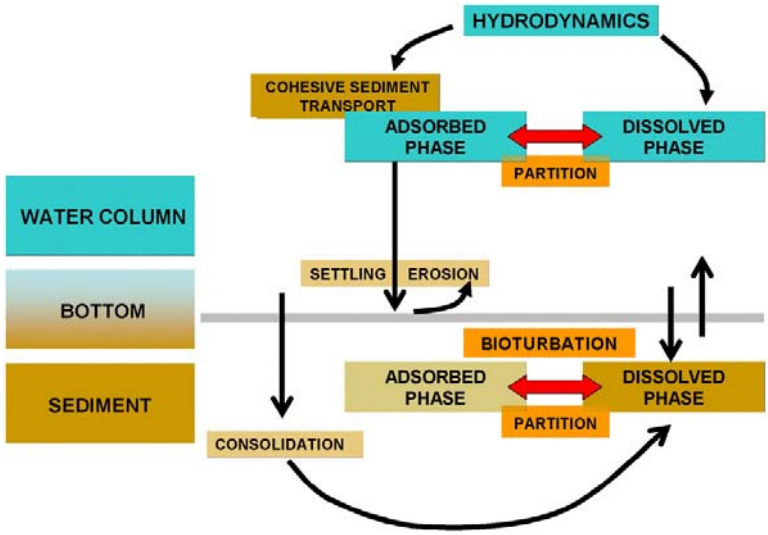

Figure 6 – Contaminant transport processes included in MOHID

Thus, currently MOHID is constituted by a water column model, which is composed by a free surface three-dimensional baroclinic hydrodynamic module, a turbulence module,

an eulerian transport module, a lagrangian transport module, an oil dispersion model and three biogeochemical modules; a sediment model is composed by a saturated one-dimensional consolidation model, an eulerian transport model and by a biogeochemical model; and an atmospheric processes module where atmospheric observed data or atmospheric model results can be used as forcing.

2.2.1 Water column model

Hydrodynamics

The hydrodynamic class solves the primitive continuity and momentum equations for the surface elevation and 3D velocity field for incompressible flows, in orthogonal horizontal coordinates and generic vertical coordinates, assuming hydrostatic equilibrium and Boussinesq approximation. The mass and momentum evolution equations are:

$$\frac{\partial u_i}{\partial x_i} = 0$$

$$\frac{\partial u_1}{\partial t} + \frac{\partial \left(u_j u_1\right)}{\partial x_j} = -fu_2 - g\frac{\rho_\eta}{\rho_0}\frac{\partial \eta}{\partial x_1} - \frac{1}{\rho_0}\frac{\partial p_s}{\partial x_1} - \frac{g}{\rho_0}\int_z^\eta \frac{\partial \rho'}{\partial x_1} dx_3 + \frac{\partial}{\partial x_j}\left(A_j \frac{\partial u_1}{\partial x_j}\right)$$

$$\frac{\partial u_2}{\partial t} + \frac{\partial \left(u_j u_2\right)}{\partial x_j} = fu_1 - g\frac{\rho_\eta}{\rho_0}\frac{\partial \eta}{\partial x_2} - \frac{1}{\rho_0}\frac{\partial p_s}{\partial x_2} - \frac{g}{\rho_0}\int_z^\eta \frac{\partial \rho'}{\partial x_2} dx_3 + \frac{\partial}{\partial x_j}\left(A_j \frac{\partial u_2}{\partial x_j}\right)$$

$$\frac{\partial p}{\partial x_3} = -\rho g$$

Where u_i are the velocity vector components in the Cartesian x_i directions, η is the free surface elevation, f the Coriolis parameter, A_i the turbulent viscosity and p_s is the atmospheric pressure. ρ is the density and ρ' its anomaly.

Density is computed depending on salt, temperature and pressure, by the UNESCO equation of state (UNESCO, 1981).

The model uses an ADI (Alternate Direction Implicit) time discretization scheme which minimizes stability restrictions, and is defined in an Arakawa-C type grid. Turbulence is computed through a set of available models:

- Horizontal turbulence - Constant, Smagorinsky (1963), Proportional to depth and to the square of velocity;

- Vertical turbulence – Constant, Nihoul (1984), Leendertse and Liu (1978), Backhaus and Hainbucher (1987), Pacanowski and Philander (1981), and GOTM (Burchard et al, 1999) – http://www.gotm.net, a turbulence models library coupled with MOHID, including a k-ε model and Mellor-Yamada second order turbulent closure model (Mellor and Yamada, 1982).

In the bottom, shear stress can be computed with the assumption of a logarithmic velocity gradient:

$$\tau = \rho C_d \left|\vec{u}_+\right| \cdot \vec{u}_+ \qquad C_d = \left[\frac{k}{\ln\left(\frac{z_+ + z_0}{z_0}\right)} \right]^2$$

Where τ is the bottom shear stress, u_+ is the velocity field at a distance z_+ above the bottom, C_d is the roughness coefficient, k is the Von Karman constant and z_0 is the bottom roughness length.

In the free surface, momentum flux can also be imposed in the form of shear stress.

Momentum, mass and heat transport is computed using a generic 3D advection-diffusion library including various advection schemes namely: first, second and third order upwind, centred differences and TVD (Total Variation Diminishing). Advection is solved in the three directions as a one-dimensional case and various time discretizations can be combined: explicit, semi-implicit or fully implicit.

Dissolved properties transport in the water column

Transport phenomena in the water column for a given property (P), can be described by the 3D advection-diffusion differential equation:

$$\frac{dP}{dt} = \frac{\partial P}{\partial t} + u_j \frac{\partial P}{\partial x_j} = \frac{\partial}{\partial x_j}\left(k_\Theta \frac{\partial P}{xj}\right) + (Sources - Sinks)$$

P is the concentration (ML^{-3}), j is the index for the correspondent Cartesian axis (x_1, x_2, x_3) or (x,y,z), K_Θ is the turbulent mass diffusion coefficient (horizontal/vertical). Sources and sinks related to reaction processes taken place inside the assumed control volume, which undertakes local production and destruction terms.

Particulate properties transport in the water column

Particulate properties transport is governed by a 3D advection-diffusion equation where the vertical advection includes the particle settling velocity.

$$u_Z = u_{Z'} + w_S$$

Where u_z is the overall vertical velocity of the particulate property, $u_{z'}$ is the vertical current velocity, and w_s is the property's settling velocity. This methodology enables to compute particulate properties transport, like particulate contaminants or particulate organic matter, likewise and dependent of cohesive sediments.

Two different approaches are followed to compute settling: a constant settling velocity and a cohesive sediment concentration dependent settling velocity. In the first case, each particulate can have its specific and constant settling velocity, which can be derived from literature (depending on its size and biogeochemical characteristics). The latter approach, however, needs some considerations. As the settling velocity algorithm was developed for cohesive sediment modelling, how can the other particulate properties settling velocity be computed? In this study, it is considered that it is the same as the cohesive sediment settling velocity, therefore reinforcing the importance of cohesive sediments in the distribution and fate of the adsorbed contaminants fraction. The algorithm follows formulation widely used in literature (e.g. Mehta, 1988), where the general correlations for the settling velocity in the flocculation range are:

$$W_S = K_1 C^m \qquad \text{for} \quad C < C_{HS},$$

and in the hindered settling range is:

$$W_S = K_1 C_{HS}{}^m \left[1.0 - K_2 \left(C - C_{HS}\right)\right]^{m_1} \qquad \text{for} \quad C > C_{HS}$$

where W_S (ms^{-1}) is the settling velocity, C (kgm^{-3}) is the concentration, and the subscript HS refers to the onset of the hindered settling (of about 2 to 5 kgm^{-3}). The coefficients K_1 ($m^4kg^{-1}s^{-1}$) and K_2 (m^3kg^{-1}) depend on the mineralogy of the mud and the exponents m and m_1 depend on particle size and shape.

Adsorption/Desorption

Adsorption and desorption are considered as a reaction process, that can be included in the sinks and sources terms of contaminants transport equation. This reaction involves the dissolved and the particulate phases of the contaminant being simulated, where the two phases tend to an equilibrium, which is given by a partition coefficient. The equilibrium can be described by the following system of equations (Hayter and Pakala, 1989)

$$\frac{\partial C_d}{\partial t} = k\left((D\% \times C_p - P\% \times C_d\right)$$

$$\frac{\partial Cp}{\partial t} = k\left((P\% \times C_d - D\% \times C_p\right)$$

C_p and C_d are the particulate and dissolved contaminant concentrations respectively; k (s^{-1}) is the equilibrium kinetic rate for adsorption-desorption between dissolved and particulate phase; D% is the dissolved contaminant fraction; and P% the particulate contaminant fraction.

The kinetic constant defines the rate at which the two phases tend to equilibrium. To account for the fact that, in the presence of low suspended matter concentrations, the adsorption process is less probable to occur (the probability of a contaminant ion to hit a particle is lower), a direct relation between the kinetic rate and the suspended particulate matter was implemented, where:

$$\begin{cases} k = k_{ref} \cdot \dfrac{C_{SPM_{reference}}}{C_{SPM}} & for \quad \dfrac{C_{SPM_{reference}}}{C_{SPM}} < 1 \\ k = k_{ref} & for \quad \dfrac{C_{SPM_{reference}}}{C_{SPM}} \geq 1 \end{cases}$$

2.2.2.Water-sediment interface model

The water sediment interface model computes and manages boundary conditions for the water column and sediment compartments.

Cohesive sediments fluxes

For cohesive sediments at the bottom, a flux term, F_b, (mass of sediment per unit bed area per unit time) can be defined, corresponding to a source or sink for the suspended particulate matter in conditions of erosion or deposition, respectively (Fig. 7). Consequently, at the bottom:

$F_b = F_E - F_D$

where F_E and F_D are respectively the erosion and deposition fluxes.

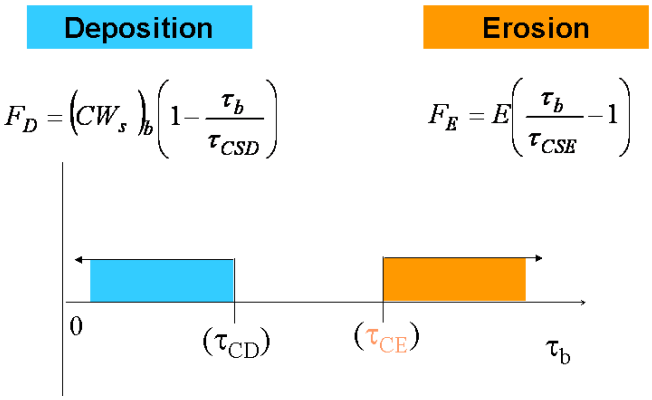

Figure 1 – Erosion and deposition modelling algorithm

It is assumed that, when bottom shear stress is smaller than a critical value for deposition, there is addition of matter to the bottom, and, when the bottom shear is higher than a critical value, erosion occurs. Between those values, erosion and deposition balance each other. The erosion algorithm used is based on the classical approach of Partheniades, (1965). Erosion occurs when the bottom shear stress exceeds the threshold of erosion. The flux of eroded matter is given by:

$$\begin{cases} F_E = E\left(\frac{\tau}{\tau_E}-1\right) & for \quad \tau_b > \tau_{CSE} \\ F_E = 0 & for \quad \tau_b < \tau_{CSE} \end{cases}$$

where τ is the bed shear stress, τ_{CSE} is a critical shear stress for erosion and E is the erosion parameter ($kgm^{-2}s^{-1}$). This erosion algorithm is computed at the sediment-water interface (fluff-layer). If this layer is eroded, erosion occurs from the underlying sediment layer, which has a higher level of compaction, therefore increasing the erosion shear stress thresholds. This is obtained by defining τ_{CSE} as depth dependent, reflecting the increasing resistance of the sediment to be eroded as scouring reaches deeper layers.

Wave induced shear stress can also be computed by the model by a linear wave theory, given wave characteristics such as wave period and wave significant height. Estuarine local waves can be important in terms of sediment resuspension, especially in shallow water where the wave stresses effect reaches the sediment bed. Pina (2001), presents a detailed description on the formulation implemented in the model.

On the other hand, the deposition flux can be defined as:

$$F_D = -p(W_S C)_b$$

where p is the probability of sediment particles to set down on the bed; W_S is near-bed the settling velocity; and C the near-bed cohesive sediment concentration. The probability of deposition (Krone, 1962), can be defined as:

$$p = (1 - \frac{\tau_b}{\tau_{CSD}})$$

where τ_b (Pa) and τ_{CSD} (Pa) are the bottom shear stress and the critical shear stress for deposition respectively. This concept reflects the fact that the deposition of flocks is controlled by near-bed turbulence. For a flock to stick to the bed, gravitational forces must be strong enough to withstand the near bed shear stress. The deposition algorithm (Krone, 1962), like the erosion algorithm, is based on the assumption that deposition and erosion never occur simultaneously, i.e. a particle reaching the bottom has a probability of remaining there that varies between 0 and 1 as the bottom shear stress varies between its upper limit for deposition and zero respectively. Deposition is calculated as the product of the settling flux and the probability of a particle to remain on the bed:

$$\begin{cases} F_D = (CW_S)_B(1 - \frac{\tau}{\tau_{CSD}}) & for \quad \tau_b < \tau_{CSD} \\ F_D = 0 & for \quad \tau_b > \tau_{CSD} \end{cases}$$

The critical shear stress for deposition depends mainly on the size of the flocks. Bigger flocks have higher probability of remaining on the bed than smaller flocks. As a single characteristic class of cohesive sediment is considered in the model, parameters must subject to calibration, starting from reference values found in literature, in order to achieve good approximations in the final results.

Consolidation, in this study, was considered to occur on recently deposited sediments at the sediment-water interface, and was modelled as a sediment flux, $F_{consolidation}$ ($kg_{sed}m^{-}$

$^{2}s^{-1}$), between the fluff layer and the first sediment layer at a certain rate, $k_{consolidation}$ (s^{-1}), dependent on the sediment mass per unit of area deposited at the fluff layer. It is assumed that consolidation only occurs when shear stress (τ_b) is lower than the critical shear stress for deposition (τ_{CSD}).

$$\begin{cases} F_{consolidation} = 0 & \tau_b < \tau_{CSD} \\ F_{consolidation} = M_{sediment} \cdot k_{consolidation} \end{cases}$$

This consolidation flux is one of the governing processes for particulate contaminant fractions to enter the sediment compartment.

Particulate properties fluxes

Particulate properties fluxes at the sediment-water interface depend on erosion and on consolidation processes.

As the erosion algorithm was developed specifically for cohesive sediment modelling, when computing other particulate properties fluxes at the bed, the erosion rate parameter cannot be the same. Thus, a specific proportionality factor for the erosion constant is computed, E_{prop}, for each property, relating the quantity of property ($M_{property}$ – $kg_{property}m^{-2}$) to the quantity of cohesive sediment deposited in the bed ($M_{sediment}$ – $kg_{sed}.m^{-2}$). The particulate property erosion flux is then computed similarly to cohesive sediments but with a specific E_{prop}.

$$E_{prop} = E\left(\frac{M_{property}}{M_{sediment}}\right)$$

This way, critical shear stress values are considered equal for all particulate properties, being the specific erosion constant the differentiating factor.

When consolidation occurs, a similar algorithm is followed, relating the sediment consolidation flux with the particulate property deposited mass. Thus, the property consolidation flux (F^{prop}) can be computed as in the following expression:

$$F^{prop}_{consolidation} = F^{sediment}_{consolidation}\left(\frac{M_{property}}{M_{sediment}}\right)$$

Dissolved properties fluxes

Dissolved properties fluxes across the water-sediment interface depend both on erosion/consolidation processes and on concentration gradients between the water column's lower layer and on the interstitial water of the sediment's upper layer.

As stated before, when the fluff-layer is active (i.e. there are recently deposited sediments on the bed), interstitial water between those sediment particles is not considered. Thus, when erosion occurs, there is no dissolved properties income from the fluff layer to the water column.

In the sediments' upper layers, interstitial water (containing solutes such as dissolved contaminant fractions, nutrients, etc) is flushed to the water column when consolidated sediment is eroded (upper sediment compartment layer). On the other hand, when consolidation occurs, water overlying the sediment bed becomes part of sediment's interstitial water. These processes constitute an additional flux of solutes to and from the water and sediment columns. Thus, a water flux (F^{water}) can be computed, corresponding to the amount of porewater dragged along with the eroded sediments or to the amount of overlying water dragged in the consolidation process:

$$F_{erosion/consolidation}^{water} = F_{Erosion/consolidation} \cdot A \cdot \phi_k \cdot \frac{1}{\rho_{sed} \cdot (1 - \phi_{kn})}$$

Where, $F_{erosion/consolidation}$ is the cohesive sediment flux ($kg_{sed}m^{-2}s^{-1}$) between the sediment-water interface and the sediments' upper layer, Φ_{kn} is the porosity in the upper (k=n) sediment layer, ρ_{sed} is the sediment dry density ($kg_{sed}m_{sed}^{-3}$) and A is the area (m^2) of the sediment-water interface. Respectively, solute fluxes are given by:

$$F_{erosion/consolidation}^{solute} = \frac{F_{erosion/consolidation}^{water} \cdot C^{solute}}{A}$$

where C is the solutes' concentration ($kg.m_{water}^{-3}$) in the sediment upper layer or in the water column bottom layer, depending on the type of flux (erosion or consolidation).

As mentioned above, the concentration gradients between the water column bottom layer and the sediment surface layer can also produce a mass flux through the sediment-water interface. Solutes, in a turbulent flow can be transported by a mean advective flux, turbulent diffusion and molecular diffusion. It is usually considered that solutes diffusion coefficient is equal to the fluids' turbulent viscosity, which is normally several orders of magnitude higher. Nonetheless, when approaching the sediment bed, water flow is reduced, as well as turbulent movements, leading to the increase of molecular

diffusion importance in relation with the turbulent one. Thus, a sub-diffusive layer (Boudreau, 1997) is formed, where a linear concentration gradient can be considered, and a diffusive flux, $F_{diffusive}$ ($kg_{solute}m^{-2}s^{-1}$), can be computed representing the rate at which this gradient tends to be eliminated:

$$F_{diffusive} = \frac{D_{molecular}}{\delta} \cdot A \cdot (C_{water} - C_{interstitial})$$

In which $D_{molecular}$ is the molecular diffusion coefficient (m^2s^{-1}), and δ (m) is the sub-diffusive boundary layer thickness, which is dependent on near-bed turbulence:

$$\delta = \frac{2 \cdot \nu_{water}}{u_+}$$

Where υ_{water} is the water cinematic viscosity (m^2/s) and u_+ is near-bed shear velocity (m/s).

2.2.3. Sediment column model

The sediment column model is basically a set of 1D vertical models defined below the 3D water column model. Both models share the same horizontal discretization, but compute independent vertical coordinates. As referred above, the sediment column model was in practice based on the water column strategy, and constitutes the core of the advances made in the framework of this study.

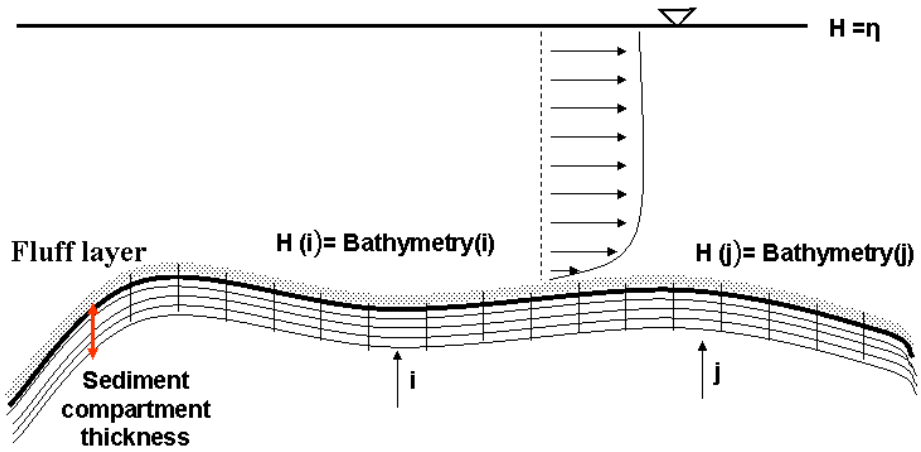

Figure 2 – Sediment compartment discretization

Sediment physical processes and properties

The sediment compartment is constituted by a module which computes the sediment geometry (variations due to erosion and consolidation), namely dry sediment volumes and interstitial water volumes. In terms of vertical referential, it is located below the water column until a certain defined depth. The construction of the domain is made by means of a depths file, similar to the bathymetry for the water column model. This way, sediments' upper layer is located at the same coordinate of the water column model bathymetric value, with a certain depth, usually 10 to 30 cm (Figure 2).

This compartment is considered to be a saturated porous media, so a key variable is porosity (Φ), which represents the fraction of volume occupied by interstitial water. Porosity decreases with depth and relates to tortuosity, a parameter which reflects the influence of porous media geometry in the transport phenomena, namely diffusion. Tortuosity can be seen as an extension of the path a solute has to take in the porewater, due to the fact that, it has to follow a complex structure of micro-channels in the available spaces between sediment particles. Boudreau (1996), finds a good agreement between tortuosity and porosity:

$$T_f = 1 - \ln(\phi^2)$$

A decay of porosity can be computed, accounting for the consolidation process.

$$\frac{\partial \phi}{\partial t} = \frac{\phi_\infty - \phi}{\lambda}$$

Where Φ_∞ is the porosity of a fully consolidation sediment and λ is decay factor (s). This consolidation process has a time scale several times higher than the erosion/deposition processes and in this study is neglected. However, it is included in the model, and can be useful in long term simulations, has when consolidating, interstitial water is pushed upwards, therefore advecting solutes through the sediment column, and even through the water-sediment interface onto the overlying water column. These fluxes can also be accounted as a source of contaminants to the water column.

The sediment compartment boundary conditions were described above, and consist on the erosion and consolidation fluxes, and are controlled by the sediment-water interface module. Erosion is made, by removing material from the sediments' upper layer. As

sediment layers are being scoured, critical shear stress increases, due to the fact that sediments compaction level increases with depth. Therefore, critical shear stress can be computed such as:

$$\tau_{CSE(z)} = (\tau_{CSE(z=0)} - \tau_{CSE(z=\infty)})e^{-\frac{z}{\psi}}$$

Where z is the depth (m) and Ψ is a decay coefficient (m).

A specific new algorithm was developed to solve discretization problems of a complex vertical domain, like the sediment compartment. The vertical resolution must be high enough to solve properly the sharp concentration gradients (contaminants, organic matter, oxygen, etc) existing in estuarine sediments. Two main problems can be found: the sediment top layer is constantly eroded until it disappears; or the deposition flux is so high that the top layer thickness increases to a level that it cannot be assumed that properties inside the layer are constant. Thus, in order to handle these problems two thickness limitations were imposed: a minimum and a maximum layer thickness.

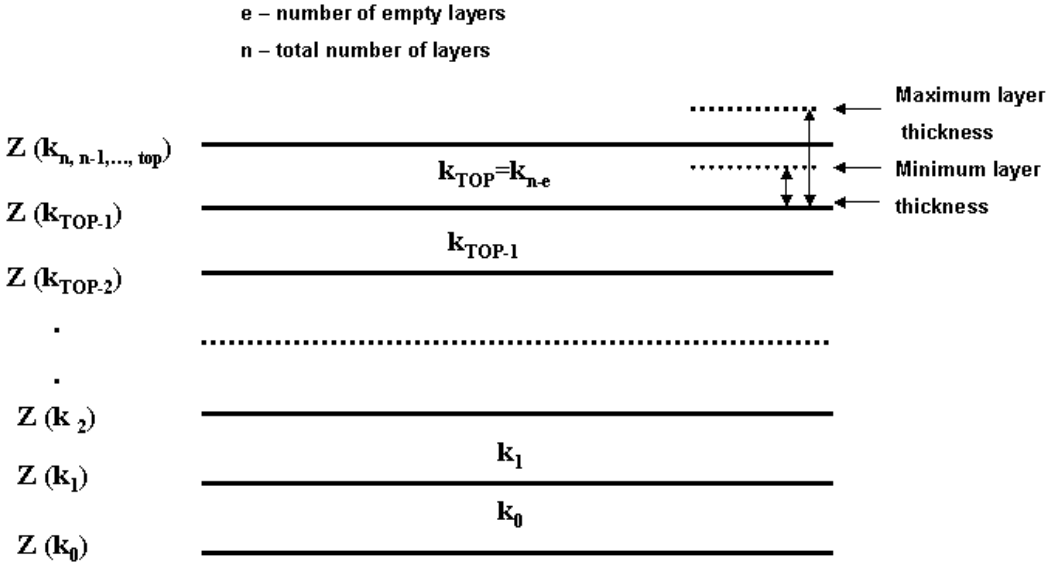

Figure 3 – Representation of the vertical discretization of a 1D sediment column.

When erosion fluxes remove material from the sediments' compartment upper layer, this flux is limited so that, in one iteration, the layer does not exceed the minimum layer thickness. When this happens, the upper layer collapses and becomes part of the lower layer, which then, becomes the top layer.

When consolidation fluxes raise the top layer thickness so that it exceeds the maximum layer thickness, a new layer is created, splitting the upper layer into two. The new upper layer is initialized has having the minimum layer thickness allowed.

To overcome these problems, a new vertical coordinate system was created to account for collapsing and splitting of layers. A two-dimensional mapping variable monitors which is the index of the top layer, above which, all water and sediment volumes are null, as well as all processes. The model must always be started with a certain number of empty top layers to account for possible creation of new layers, if consolidation occurs. If the initial number of layers is exceed, the model stops. The same happens when all sediment layers are eroded and collapsed.

The layers collapsing and splitting is followed by mass conserving algorithms applied to each of the sediment properties, both dissolved and particulate.

Dissolved properties

Transport of dissolved properties in porewater is computed only in the vertical axis, as horizontal gradients are not considered in this study. Therefore, the transport equation can be written:

$$\frac{\partial (C_d)}{\partial t} + \frac{\partial ((w) C_d)}{\partial z} = \frac{\partial}{\partial z}(k_z \frac{\partial C_d}{\partial z}) + (Sources - Sinks)$$

Where C_d is the concentration ($kg.m_{water}^{-3}$), w (m/s) is the porewater velocity due to compaction, k_z (m^2s^{-1}) is the diffusivity coefficient. The molecular diffusion coefficients must be corrected with tortuosity parameterization, to account for the increase in the solute pathways due to difficulty presented by the sediment particles for diffusion to occur. Two different formulations (Figure 4) were included in model, the first following formulation by Berner (1980), tortuosity dependent, which on the other hand is porosity dependent:

$$D_m = D_{INF} \cdot \frac{1}{T_f^{\,2}}$$

The second by Soetaert (1996), is dependent of porosity square.

$$D_m = D_{INF} \cdot \phi^2$$

Where, D_{INF} (m^2s^{-1}) is the molecular diffusion coefficient in solution, and D_m (m^2s^{-1}) is the corrected molecular diffusion coefficient.

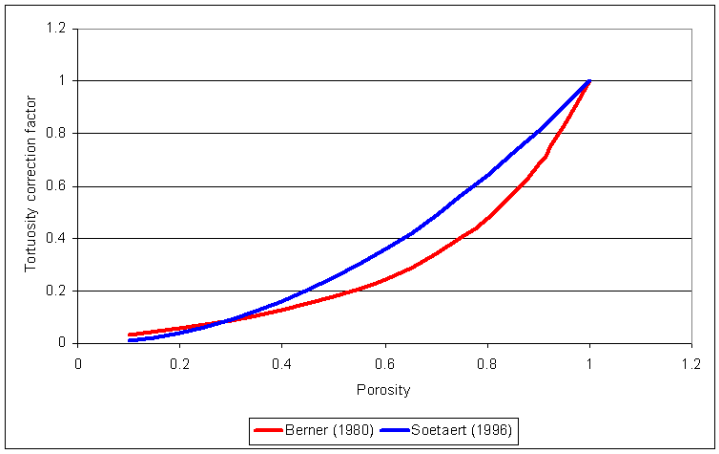

Figure 4 – Comparison between the two formulations used to compute tortuosity correction factor

Bioturbation is computed as a diffusion coefficient, which is present until a certain depth, and decreases exponentially with it. This pretends to simulate benthic fauna activity, which is most of the times present in sediments upper 10-15cm. Below this, bio-activity can be considered negligible. Thus, the bioturbation diffusion coefficient (Fig.11), D_b (m^2s^{-1}), can be computed by:

$$D_b = \begin{cases} D_b & for\ z < z_b \\ D_b \cdot e^{\frac{-z-z_b}{\alpha}} & for\ z > z_b \end{cases}$$

In which z_b is the depth limit for maximum biological activity and α is a decay coefficient (m) to account for the decrease of bioturbation with depth.

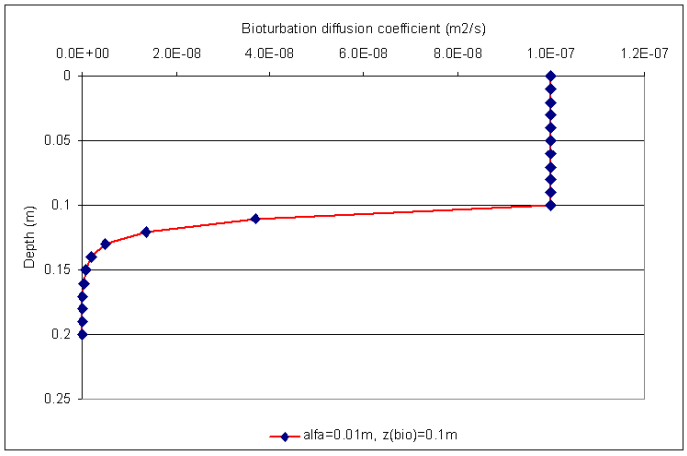

Figure 11 - Bioturbation diffusion coefficient decay with depth

Thus, the diffusivity coefficient, k_z, becomes the sum of the molecular and bioturbation diffusion coefficients:

$$K_z = D_m + D_b$$

Particulate properties

Particulate properties ($kg_{property}/kg_{sediment}$) vary in time due to sinks and sources, namely adsorption/desorption, and due to bioturbation mixing effect.

$$\frac{\partial (C_p)}{\partial t} = \frac{\partial}{\partial z}(D_b \frac{\partial C_p}{\partial z}) + (Sources - Sinks)$$

Adsorption/Desorption

Adsorption and desorption processes are simulated with a similar approach as in the water column.

2.2.4 Adapting the model for the annular flume scale

MOHID was originally designed as an estuarine, coastal and ocean model. In order to apply the model at the annular flume scale some new developments had to be made in order to adapt it. Although based in Navier-Stokes equations, the applicability of the model to such a small scale is discussable, as the turbulence parameterization may not be adequate, as well as the assumption of the hydrostatic hypothesis. A non-hydrostatic version of MOHID has recently been developed and might provide, in the future, an important step to improve the characterization of the complex flow patterns developed in the annular flume.

Nevertheless, and taking into account model limitations, an application was setup in order to simulate flow in the annular flume, using the following new features:

- centrifugal acceleration inclusion in the inertial forces term when computing the hydrodynamic solution;
- circular horizontal discretization;

Centrifugal acceleration

A centrifugal acceleration term was introduced in the model as function of the radius of the annular flume.

$$a_{centrifugal} = \frac{u^2}{r}$$

Where u is the radial velocity and r is the distance to the centre of the flume. This term is added to the inertial forces term.

Circular horizontal discretization

A new type of coordinate was introduced in order to define the circular geometry of the flume. The coordinates are constructed into a referential in which the centre of the annular flume is the origin (Fig. 12). Considering a number of grid cells in the radial axis with a defined spacing (dx) and the angles (θ_i) in which to divide the circle, a full discretization is accomplished. A second origin point must be given in order to define the inner radius of the flume. The outer radius is computed by the sum of the distances (dx) in the radial axis.

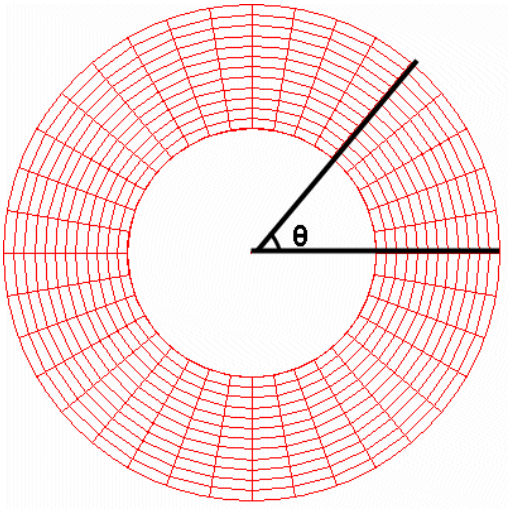

Figure 12 – Horizontal circular coordinates

3. Results

3.1. Laboratory experiments

3.1.1. Sediment properties

Tables 5 to 8 summarize surface and depth-averaged biogeochemical properties of the sediment before the erosion runs. (tables 5 and 6, manipulated sediment; tables 7 to 8 undisturbed sediment). When not measured directly, mud content, water content and bulk density were calculated using expressions in Flemming and DelaFontaine, 2000.

Shear strength (measured with the fall-cone), organic matter and copper content profiles are presented in figures 13, 14 and 15.

Sediment chlorophyll *a* and pheopigments profiles are presented in figures 16 and 17. Figures 18 and 19 show saline and EDTA extracted EPS profiles in the sediment for the four treatments (all profiles were measured in EXP2).

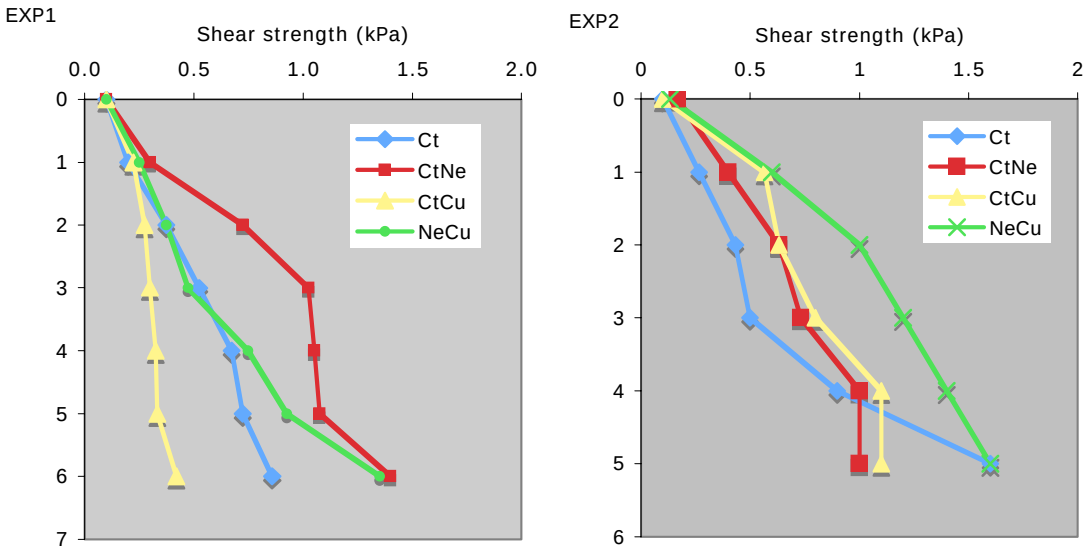

Figure 13 – Shear strength profiles (fall-cone, kPa) in the four treatments with manipulated (EXP1) and undisturbed sediments (EXP2). (standard deviation is not represented for clarity)

Table 5. Biogeochemical properties of the surface (0-5mm) of the **manipulated sediment** before erosion. (average±st. dev., n=3)

	Dry bulk density (gcm^{-3})	Mud content (%)	Shear strength (kPa)	Organic matter (%)	Water content (%)	Copper ($mg\ Kg^{-1}$)
CT	0.389	95	0.1 ±0.0	10.79±0.2	66.96	31.3±3.1*
CTNE	-	-	0.2±0.1	9.75±0.5	-	31.3±3.1*
CTCU	0.309	96.9	0.1±-0.0	10.59±0.7	72.07	175.72±0.9
NECU	0.319	95.8	0.1±0.0	11.15±2.1	71.36	167.03±2.3

* from previous studies

Table 6. Biogeochemical properties of the **manipulated sediment** before erosion, depth averaged values for the 0-35mm and 35-80mm layers, and for the whole sediment (average ± stdev, n=3)

	Depth	Dry bulk density (gcm^{-3})	Mud content (%)t	Shear strength (kPa)	Organic matter (%)	Water content (%)	Copper ($mg\ Kg^{-1}$)
	0-35mm	0.373±0.02	89.8	0.3±0.2	9.87±0.2	67.73	
CT	35-80mm	0.355±0.00	91.8	0.75±0.1	9.06±0.3	68.91	31.3±3.1*
	0-80mm	0.367±0.02	90.5	0.49±0.3	9.56±0.8	68.12	
	0-35mm	-	-	0.54±0.4	9.27±0.5	-	
CTNE	35-80mm	-	-	1.18±0.2	9.15±0.3	-	31.3±3.1*
	0-80mm	-	-	0.81±0.5	9.22±0.4	-	
	0-35mm	0.419±0.08	85	0.23±0.1	9.95±0.6	64.94±1.8	182.93±4.6
CTCU	35-80mm	0.503±0.01	76.6	0.36±0.1	7.73±1.0	59.74±0.8	196.97±5.0
	0-80mm	0.455±0.08	81.3	0.28±0.1	8.99±1.4	62.71±1.3	188.95±4.8
	0-35mm	0.429±0.09	83.9	0.30±0.2	10.52±1.0	64.34±1.5	179.72±5.8
NECU	35-80mm	0.568±0.02	70.4	1.01±0.3	7.93±1.6	56.18±1.0	187.44±5.9
	0-80mm	0.489±0.10	77.9	0.60±0.4	9.41±1.8	60.84±1.3	183.03±5.8

Table 7. Biogeochemical properties of the surface (0-5mm) of the **undisturbed sediment** before erosion. (average±st. dev., n=3)

	Dry bulk density (gcm^{-3})	Mud content (%)	Shear strength (kPa)	Organic matter (%)	Water content (%)	Chl*a* (mgm^{-2})	Pheopigments (mgm^{-2})	EPS-S (mgm^{-2})	EPS-EDTA (mgm^{-2})	Copper ($mg\ Kg^{-1}$)
CT	0.323±0.021	95.3	0.1 ±0.0	8.45±0.4	71.09±1.5	14.51±3.9	63.03±12.2	49.35±10.9	50.35±44.5	31.3±3.1*
CTNE	0.355±0.022	91.8	0.2±0.1	8.40±0.4	68.87±1.5	7.19±2.5	93.21±24.9	180.53±16.9	310.33±88.9	31.3±3.1*
CTCU	0.338±0.013	93.7	0.1±-0.0	8.38±0.3	70.08±0.9	33.89±29.3	158.6±31.5	204.98±74.5	333.56±74.5	52.74±5.7
NECU	0.320±0.015	95.8	0.1±0.0	8.83±0.3	71.34±1.1	15.9±+3.6	26.62±11.3	85.01±26.3	134.9±43.4	45.86±21.9

*from previous studies

Table 8. Biogeochemical properties of the **undisturbed sediment** before erosion, depth averaged values for the 0-35mm and 35-80mm layers, and for the whole sediment (average ± stdev, n=3)

	Depth	Dry bulk density (gcm^{-3})	Mud content (%)	Shear strength (kPa)	Organic matter (%)	Water content (%)	Chl*a* (ugg^{-1})	Pheopigments (ugg^{-1})	EPS-S (ugg^{-1})	EPS-EDTA (ugg^{-1})	Cu (ugg^{-1})
CT	0-35mm	0.340±0.025	93.4	1.98±1.0	8.99±0.4	69.93±1.7	7.78±3.8	72.15±7.7	48.67±18.5	95.62±38.9	31.3±3.1*
	35-80mm	0.439±0.069	82.9	7.25±2.2	8.00±1.0	64.25±3.9	4.71±0.7	59.55±14.6	18.80±8.6	53.19±21.9	
	0-80mm	0.383±0.067	89.0	3.74±2.9	8.56±0.8	67.22±4.2	6.46±3.2	66.75±12.1	35.87±21.2	77.44±37.8	
CTNE	0-35mm	0.453±0.073	81.5	2.86±1.5	8.38±0.3	62.83±4.4	4.52±1.4	59.98±13.4	83.04±52.8	210.78±91.9	31.3±3.1*
	35-80mm	0.557±0.011	71.4	5.90±2.0	7.04±0.9	58.02±0.6	3.90±0.7	48.72±2.8	28.22±28.8	58.16±40.6	
	0-80mm	0.498±0.076	77.3	3.87±2.2	7.76±1.0	60.22±4.5	4.25±1.1	55.15±11.3	59.55±50.3	145.37±106.9	
CTCU	0-35mm	0.463±0.079	80.5	3.14±1.6	8.17±0.2	62.24±4.9	9.44±14.6	81.77±43.5	108.45±51.1	172.00±81.9	42.49±7.0
	35-80mm	0.551±0.021	72.0	6.40±2.3	7.64±0.3	58.36±1.1	4.40±0.5	43.41±3.4	29.23±22.5	80.12±66.1	43.39±3.2
	0-80mm	0.505±0.075	77.0	4.32±2.4	7.90±0.4	60.04±4.5	7.28±10.7	66.33±37.0	74.5±57.2	132.63±85.0	42.88±5.3
NECU	0-35mm	0.516±0.122	75.3	4.35±2.6	8.59±0.3	59.48±7.3	9.15±5.0	21.64±12.1	60.16±22.5	139.99±51.7	33.62±10.4
	35-80mm	0.661±0.040	62.2	8.65±1.3	8.07±0.4	53.60±1.9	2.23±1.0	33.38±2.8	80.56±16.9	120.32±46.0	34.17±5.9
	0-80mm	0.578±0.075	70.2	5.78±3.0	8.32±0.5	56.06±6.9	6.19±5.1	27.96±11.7	68.90±21.6	131.56±46.4	33.86±8.1

*from previous studies

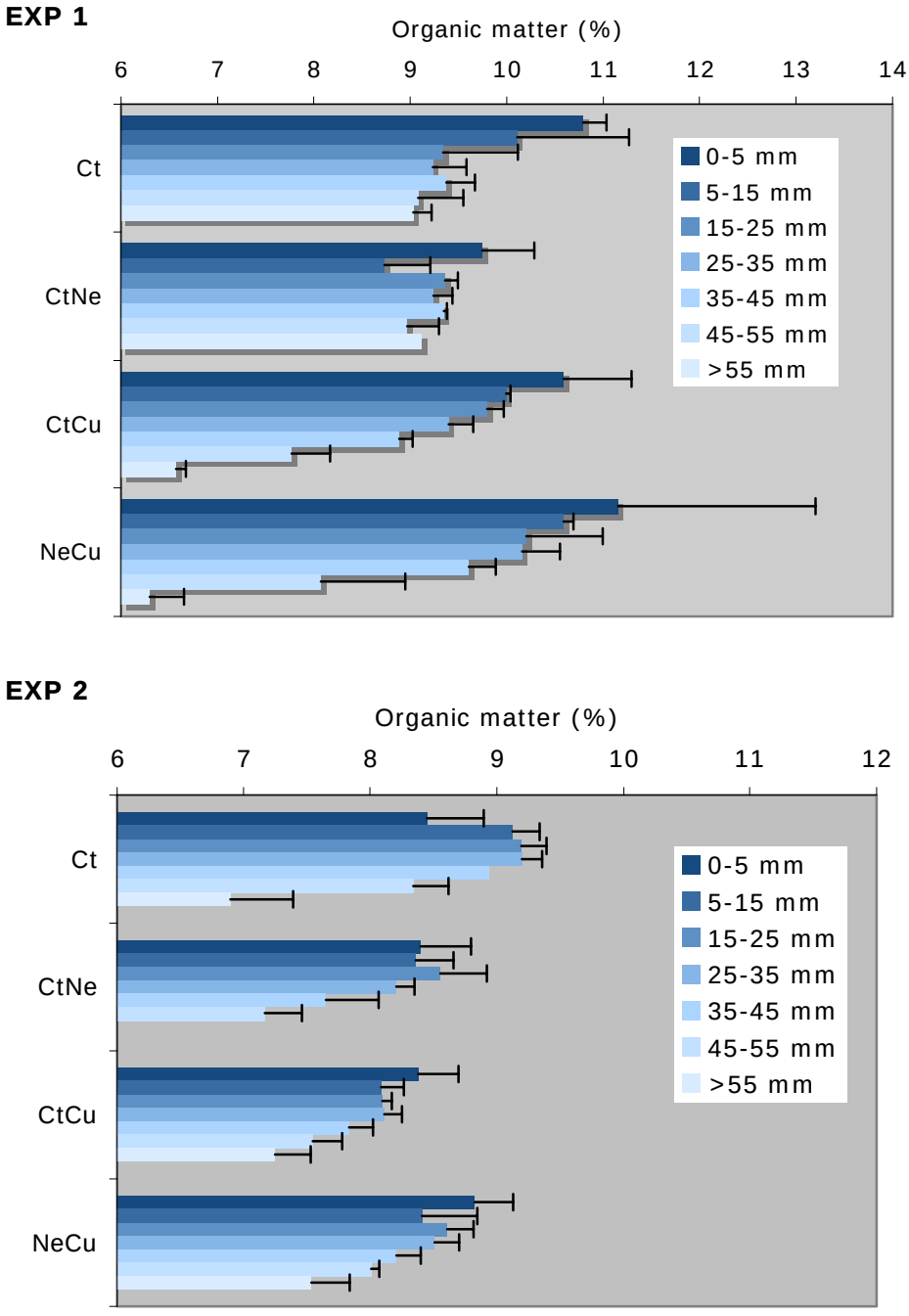

Figure 14 – Organic matter profiles (%) in the four treatments with manipulated (EXP1) and undisturbed sediments (EXP2).

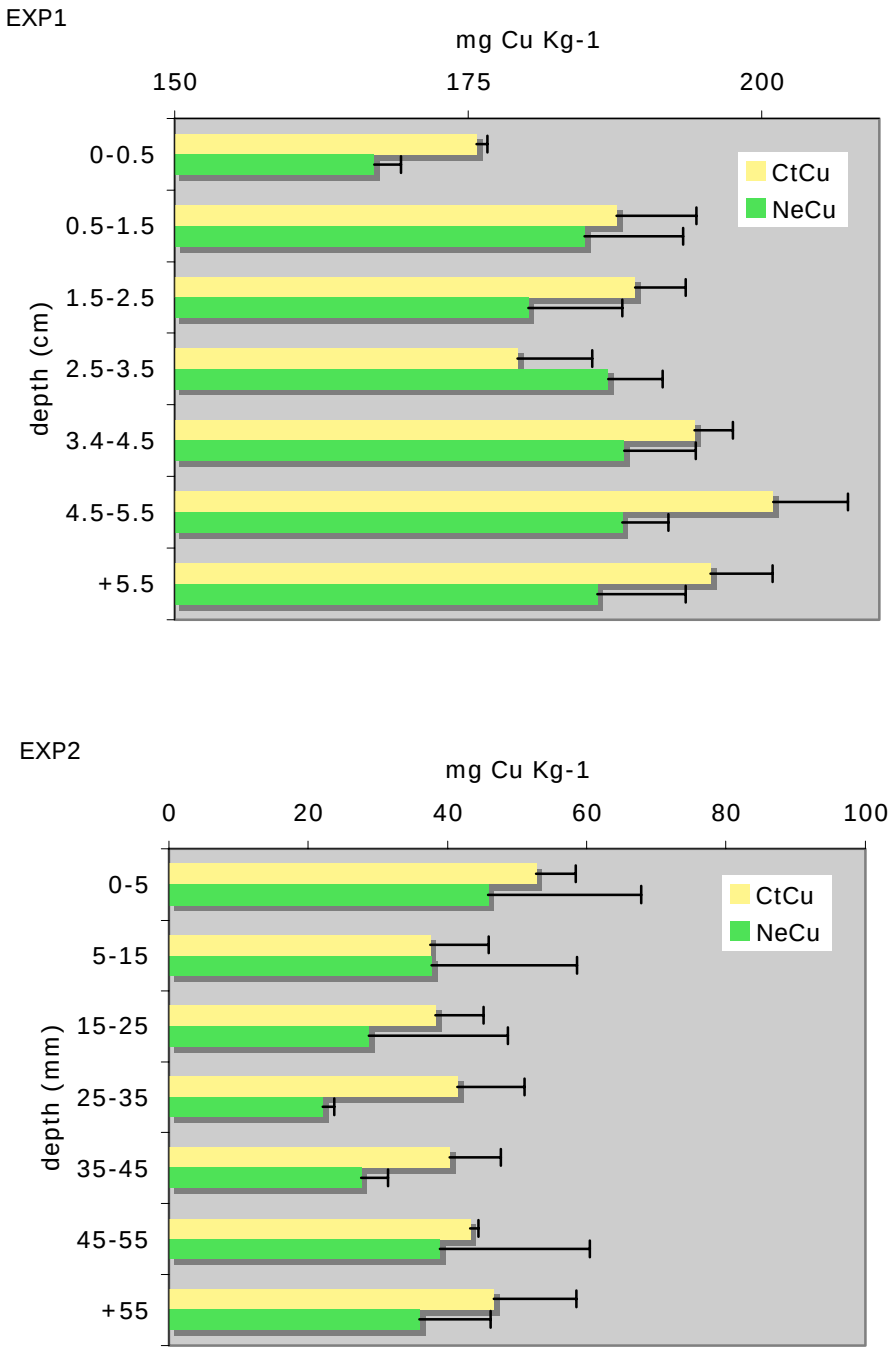

Figure 15 – Copper content profiles (mg Kg^{-1}) in the copper treatments with manipulated (EXP1) and undisturbed sediments (EXP2).

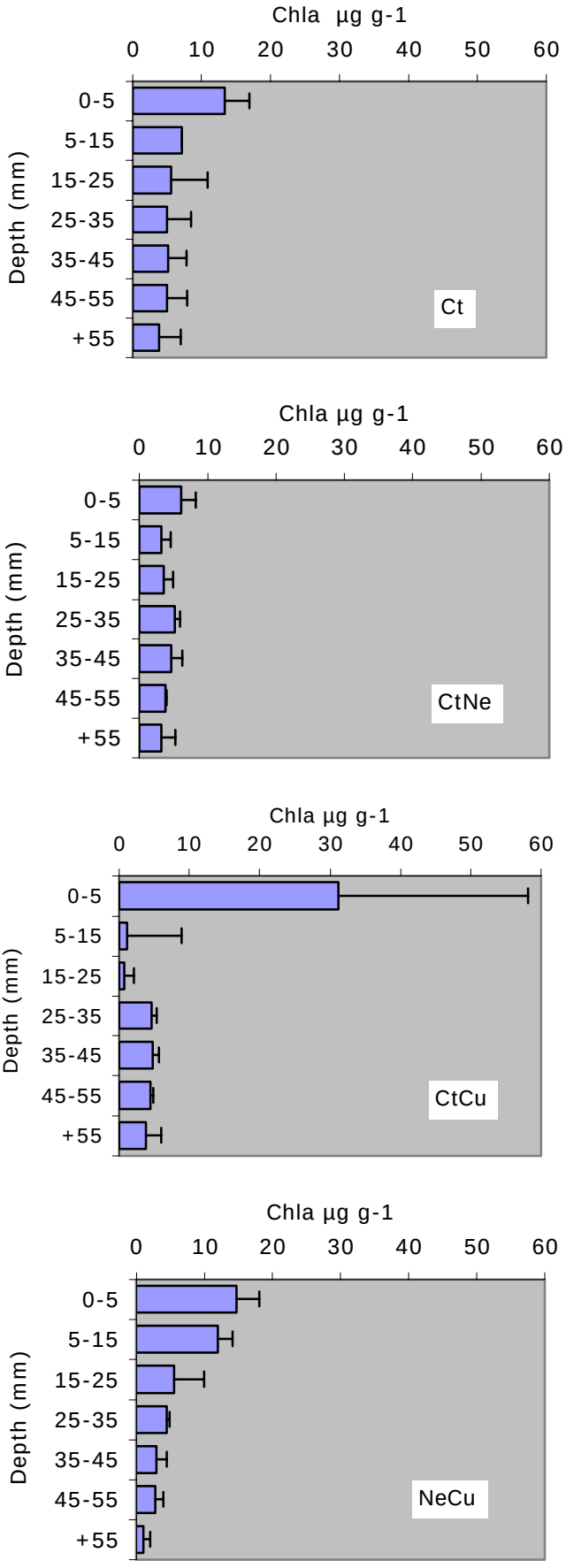

Figure 16 – Chlorophyll *a* profiles in the four treatments (EXP2).

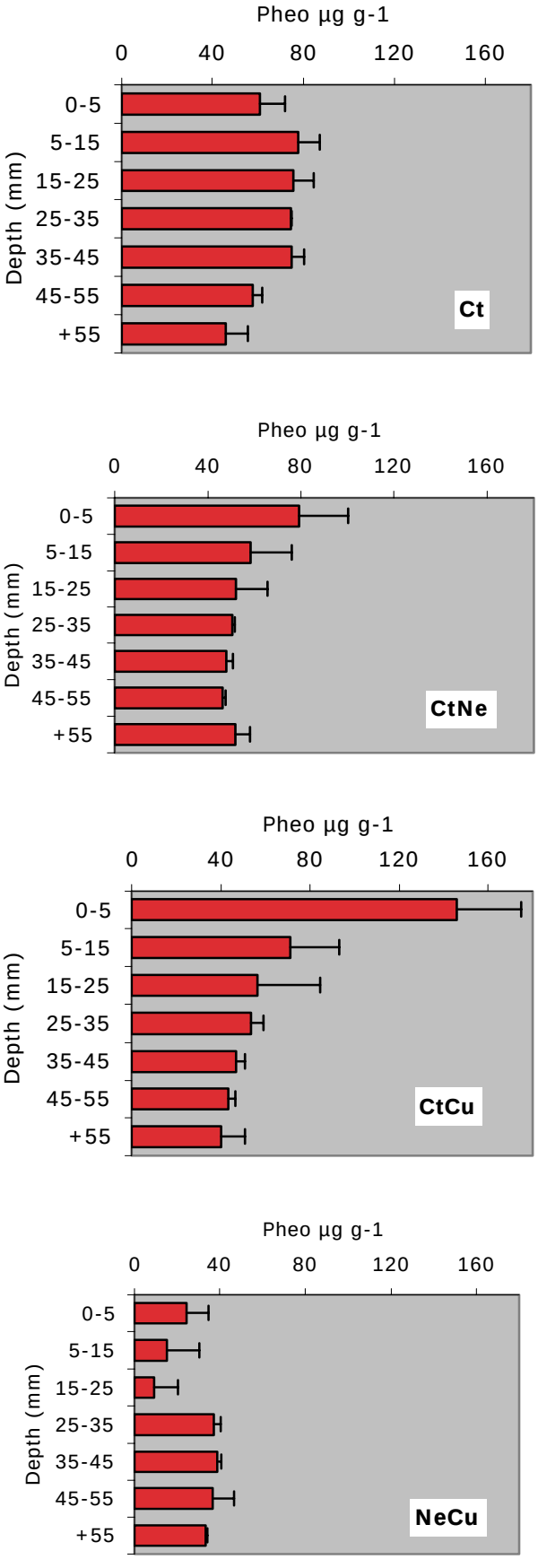

Figure 17 – Pheopigments profiles in the four treatments (EXP2).

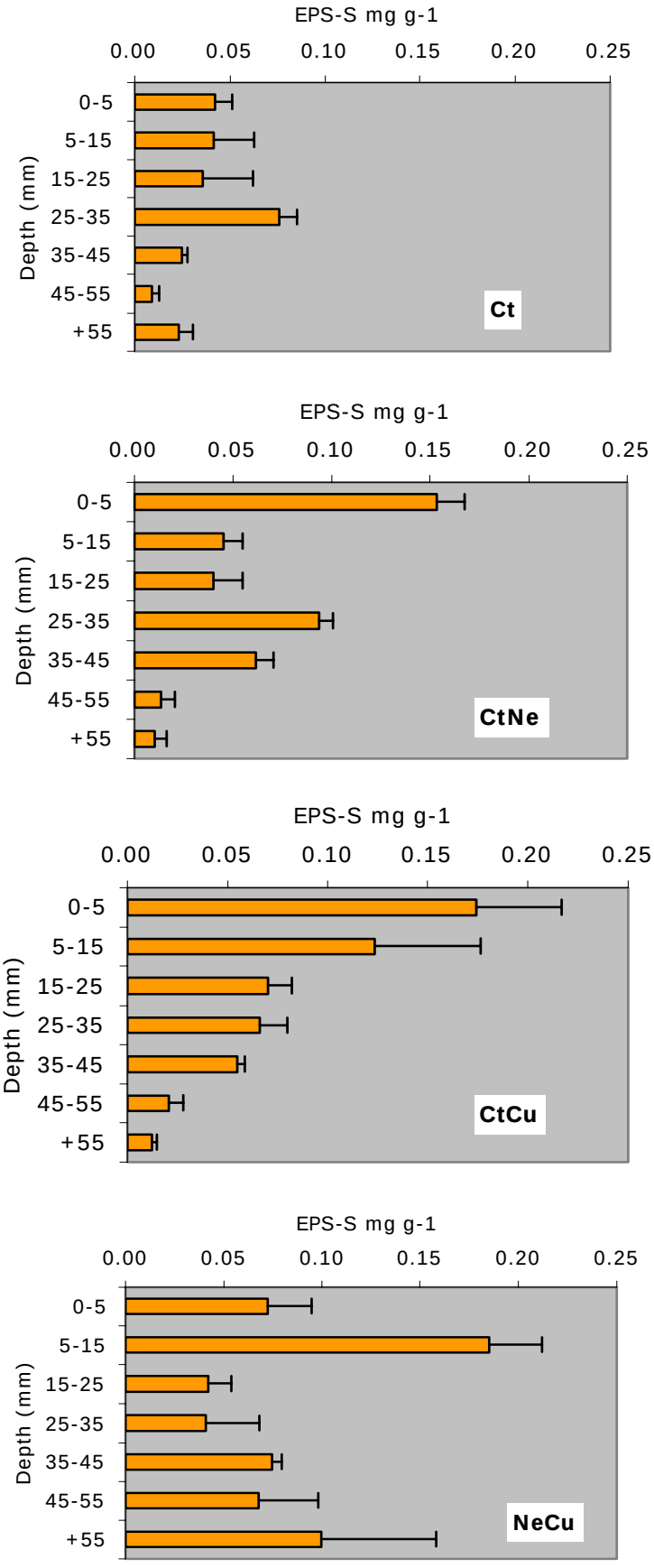

Figure 18 – Saline extracted EPS profiles in the four treatments (EXP2).

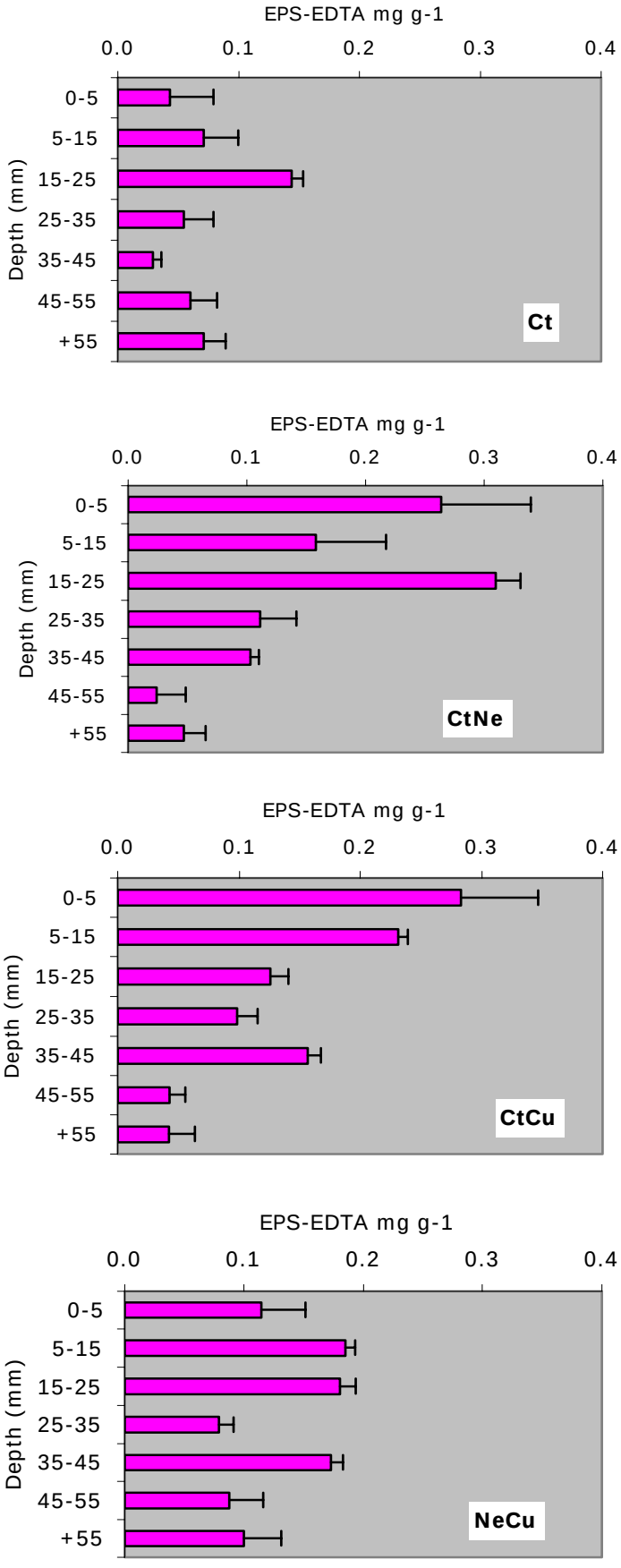

Fig. 19 – EDTA extracted EPS profiles in the four treatments (EXP2).

Manipulated and undisturbed sediments

There are large differences in the results whether considering manipulated or undisturbed sediments. These differences are present in the sediment characteristics before erosion and in the way sediment erodes with increasing water velocities.

Sediment properties before erosion we measured in a flume section kept outside the flume and may have been subjected to conditions that were not exactly the same as the sediment in the flume. Main differences were water column height, which was lower outside the flume and temperature, higher due to lights being at a shorter distance from the sediment.

Undisturbed sediments show in general higher shear strength/more compaction that manipulated ones (Fig.13), even though the latter were allowed to stabilize under laboratory conditions for 21 days after manipulation. Apparently this period of time is not enough to match natural conditions.

Mud content and organic matter (Fig. 14) are higher in the manipulated sediment since it was made of only the topmost 2cm, where mud is dominant.

N.diversicolor contributes to increase compaction especially in the deeper sediment layers. This is probably and edge effect related to the existing walls of the mesocosms, compared to the absence of physical limitations for burial in the field. In the absence of *N.diversicolor* compaction is higher in the undisturbed sediments

As expected, deeper sediment layers show higher shear strength, lower mud content, water content and organic matter.

Pigments (chlorophyll a and pheopigments) and carbohydrates (EPS-S and EPS-EDTA extractable fractions) were generally higher in the surface layers (Table 8, Figs 17-19). This is expected, as microphytobenthic communities are more abundant in those layers and diatoms are generally associated with EPS-S. Chlorophyll was present at all depths though it showed lower contents in the layers >4 cm. The high content of chlorophyll and the high variability in the contaminated sediment without N.diversicolor is not clear. In fact we would expect algal cells to die from contamination. More replicate sampling would explain if this high content is or is not a result of patchiness.

The presence of N.diversicolor reduces chlorophyll a at the surface, through sediment ingestion and dragging and burying of algal cells with the movements of the body, in and out of the galleries and over the surface, in search of food.

N.diversicolor may have contributed to an increase of pigments, EPS-S and EPS-EDTA in the deeper layers. On one hand its activity may have dragged down microphytobenthic individuals and on the other hand mucus secreted to line the walls of the galleries may have increased the EDTA extractable fraction. Contamination by copper in an early stage is likely to have increased avoidance movements and mucus secretion in the biota present, increasing therefore both EPS fractions. Pheopigments were higher in the contaminated sediments indicating degradation of conditions. Later, mortality of *N.diversicolor* (and certainly other biota not accounted for) and bacterial decay may have also contributed to the EDTA fraction (EPS-EDTA was roughly double the EPS-S fraction). Anoxia in the contaminated treatments was evident (black areas). This may have resulted from inhibition of activity and mortality caused by copper toxicity. It is not clear if bacteria were active in these conditions and would initiate decomposition.

Contamination

In what concerns contamination the main differences arise from whether the contaminant was present in the sediment or in the water (Tables 5-8, Fig.15). Manipulated sediments were contaminated by mixing and then stabilized for a period of 21 days and undisturbed sediments were exposed during 7 days to water borne contamination.

Copper added to the sediment was mostly adsorbed to particles and not bioavailable, so its accumulation and toxicity was reduced (no mortality was found)

Water-borne contamination was much more effective towards the animals due to the presence of dissolved copper readily available to the animals. This is illustrated by the higher accumulation rates (see Table 9) that result from a much shorter exposure period (7 days against 21 days) and increased mortality.

The surface sediment showed lower copper content than the deeper layers as a result of input to the overlying water (Table 6). This is not so clear when contamination was water-borne and slightly higher contents occurred at the surface (Table 8).

Bioaccumulation of copper in by *N.diversicolor* contributed to lower the copper content of the contaminated sediment (Fig .31).

Dissolved copper, measured during the flume runs before erosion with non-contaminated water, is lower in manipulated than in the undisturbed sediments. The bioaccumulation factor (relating to water concentrations before erosion) in the manipulated sediment is twice as high as the one for the undisturbed sediment. We must not forget that they refer to very different exposure periods.

3.1.2. Erosion parameters

In tables 9 to 10 critical erosion velocity (U*crit) critical shear stress eroded mass and other erosion parameters are presented for manipulated and undisturbed sediments respectively. Inputs of chlorophyll a, pheopigments and EPS from the sediment to the water column are presented in table 11.

SPM registered with the OBS in the flume during the stepwise increase in velocity in shown in figure 20.

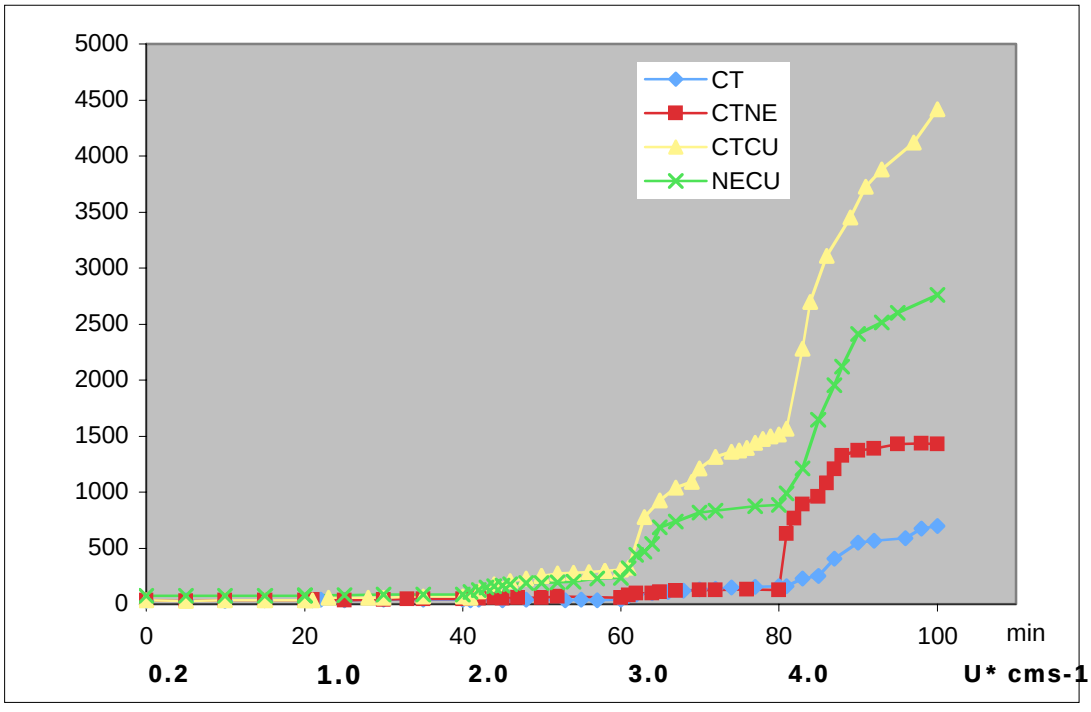

Figure 20 – Suspended particulate matter (mg l-1) measured with an OBS probe during flume runs in EXP2. Current velocity (<2 to 40cms^{-1}) was increased every 20 minutes (shear velocity U* from 0.2 to 4 cms-1).

Table 9 – Erosion parameters of the **manipulated sediment** at a current velocity of ~40cms^{-1}

	U*crit (cms^{-1})	Shear stress crit (Pa)	Eroded mass (gm^{-2})	Erosion rate (gm^{-2}s^{-1})	U* (cms^{-1})	Shear stress (Pa)	Erosion depth (mm)
Ct	6.7	4.6	199.54	0.16	8.8	7.9	0.6
CtNe	6.1	3.9	542.01	0.42	8.7	7.7	-
CtCu	6.4	4.3	317.31	0.26	9.5	9.2	1.0
NeCu	6.5	4.3	443.00	0.35	9.2	8.7	1.3

Table 10 – Erosion parameters of the **undisturbed sediment** at a current velocity of ~40cms^{-1} (U*4.1cms^{-1})

	U*crit (cms^{-1})	Shear stress crit (Pa)	Eroded mass (gm^{-2})	Erosion rate (gm^{-2}s^{-1})	Shear stress (Pa)	Erosion depth (mm)	Erosion type
Ct	2.9	0.9	200.64	0.13	1.7	0.6	I
CtNe	2.8	0.8	408.92	0.31	1.7	0.9	I
CtCu	2.1	0.5	1266.88	0.69	1.7	2.6	II
NeCu	2.1	0.4	791.08	0.45	1.7	1.5	II

Table 11. Eroded chlorophyll a and pheopigments, EPS-S and EPS-EDTA (mgm-2) and % eroded from the 0-5mm layer of the **undisturbed sediment** at ~40cms^{-1}.

	Eroded chla		Eroded pheopigments		Eroded EPS-S		Eroded EPS-EDTA	
	mgm^{-2}	% (0-5mm)	mgm^{-2}	% (0-5mm)	mgm^{-2}	% (0-5mm)	mgm^{-2}	% (0-5mm)
CT	4.73±1.8	32.5	4.13±3.9	6.6	134.22±17.8	271.99	81.56±31.8	161.9
CTNE	3.66±1.0	50.9	6.96±3.8	7.5	100.67±67.7	55.77	44.17±29.5	14.2
CTCU	3.82±1.0	11.3	49.78±26.2	31.4	69.48±13.8	33.90	99.40±18.8	29.8
NECU	3.59±1.0	22.5	18.4±4.7	69.4	33.32±8.9	39.19	86.48±50.7	64.1

3.1.3. Input of materials to the water column

Suspended particles

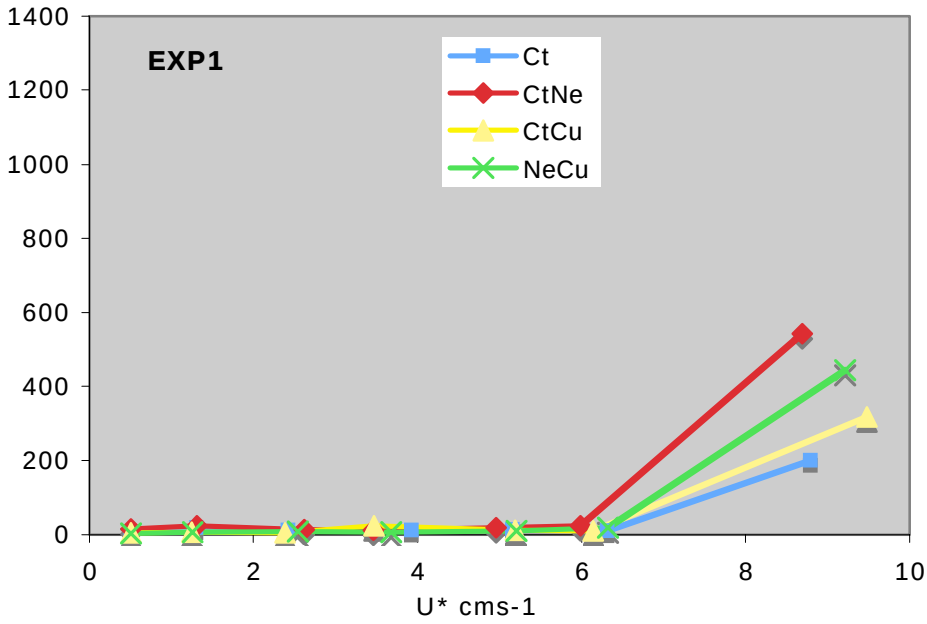

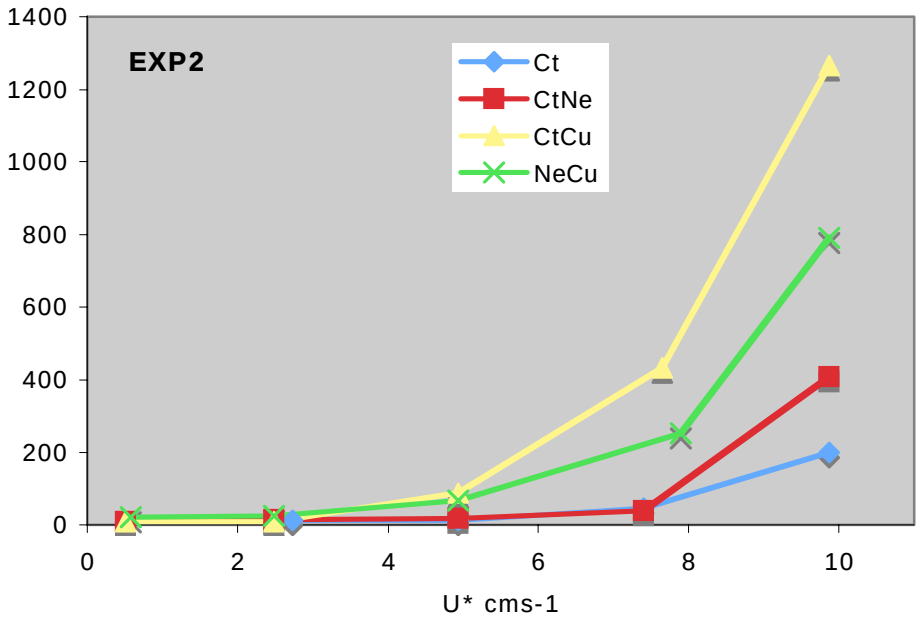

Figure 21 – Eroded mass (g m-2) as a function of shear velocity for the four treatments, with manipulated (EXP1) and undisturbed (EXP2) sediments.

Chlorophyll a and pheopigments

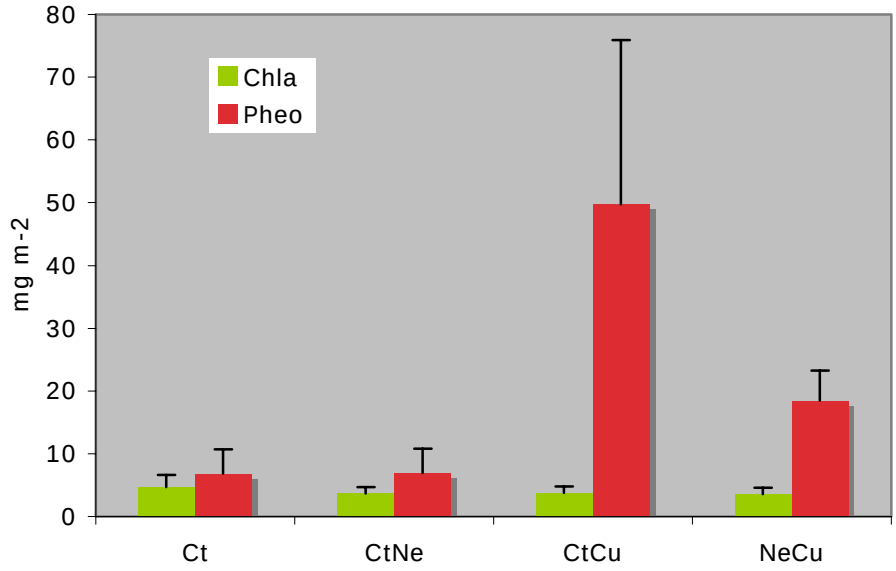

Figure 22 – Chlorophyll *a* and pheopigments in the water after 20 minutes at U* 4.1 cms^{-1} (EXP2)

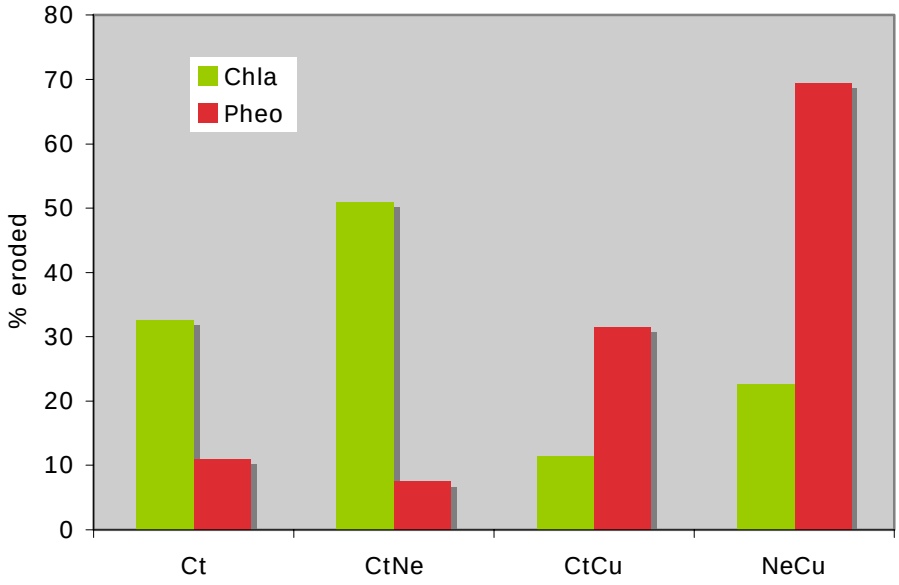

Figure 23 – Chlorophyll *a* and pheopigments (%) eroded from the 0-5mm layer (after 20 minutes at U* 4.1 cms^{-1} EXP2).

Carbohydrates (EPS)

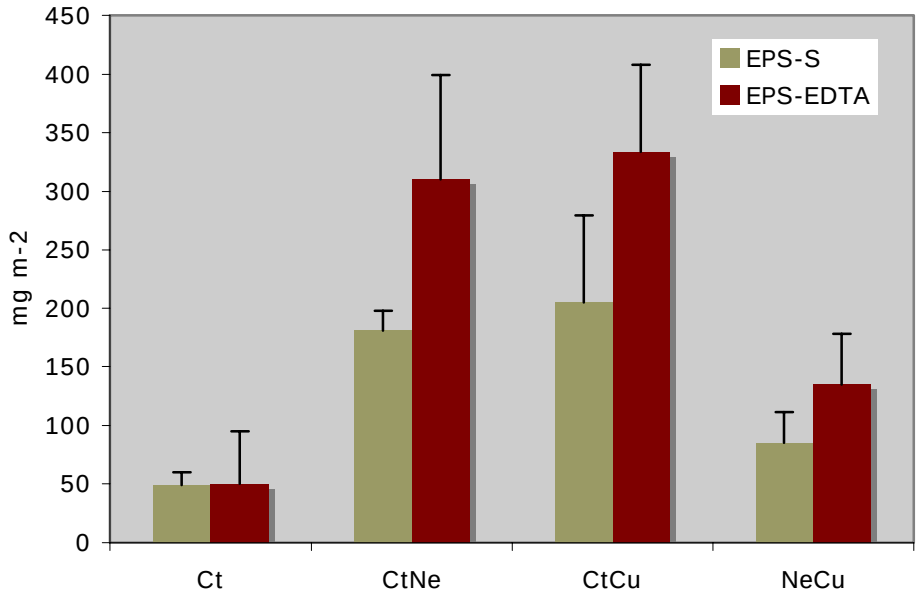

Figure 24 – Saline (S) and EDTA extractable EPS in the water after 20 minutes at U* 4.1 cms^{-1} (EXP2)

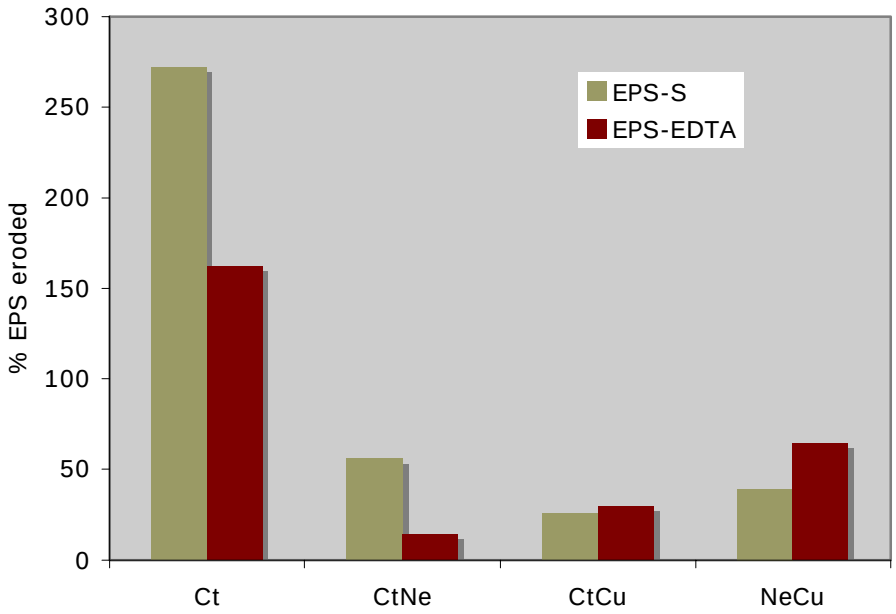

Figure 25 – Saline (S) and EDTA extractable EPS (%) eroded from the 0-5mm layer (after 20 minutes at U* 4.1 cms^{-1}; EXP2).

Copper

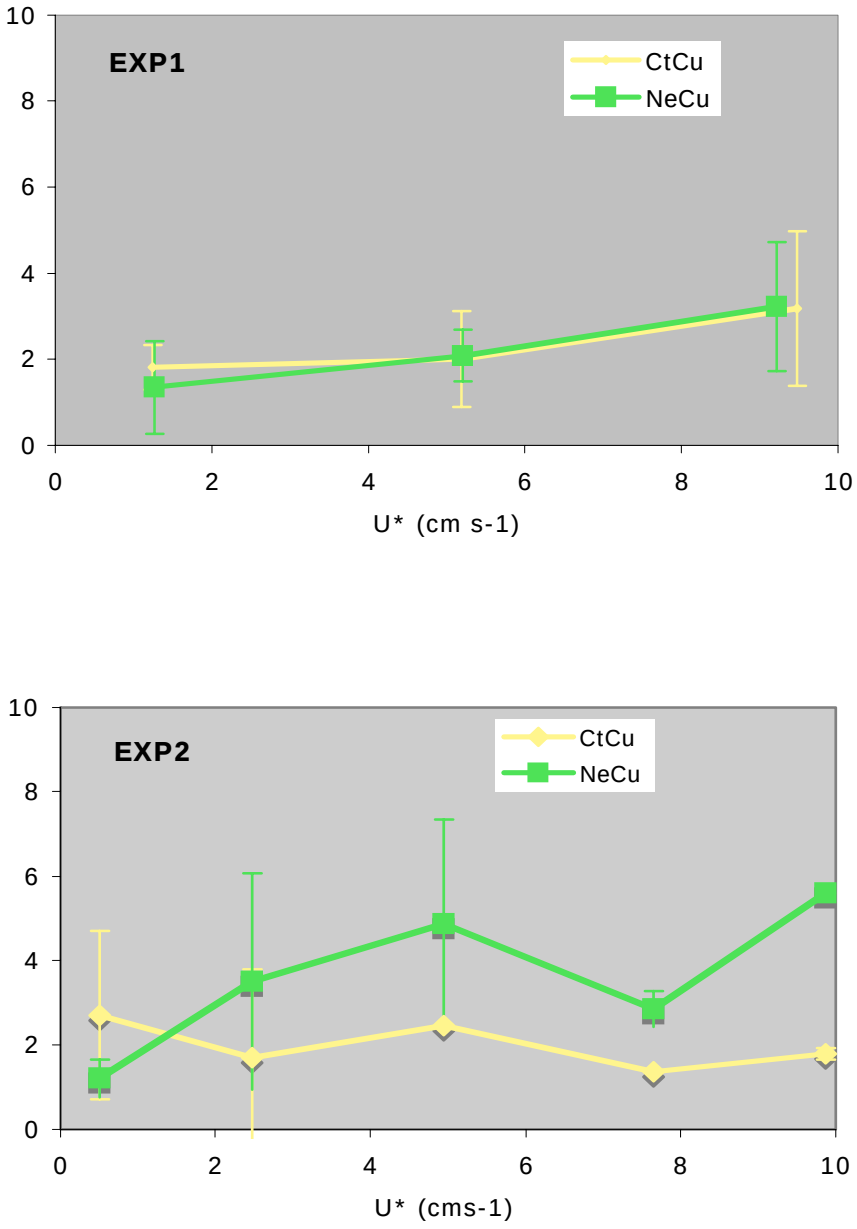

Figure 26 - Dissolved copper concentration (µg l^{-1}) with incresing shear velocity (U* cms^{-1}) in the copper contaminated treatments in EXP1 (sediment contamination) and EXP2 (water-borne contamination).

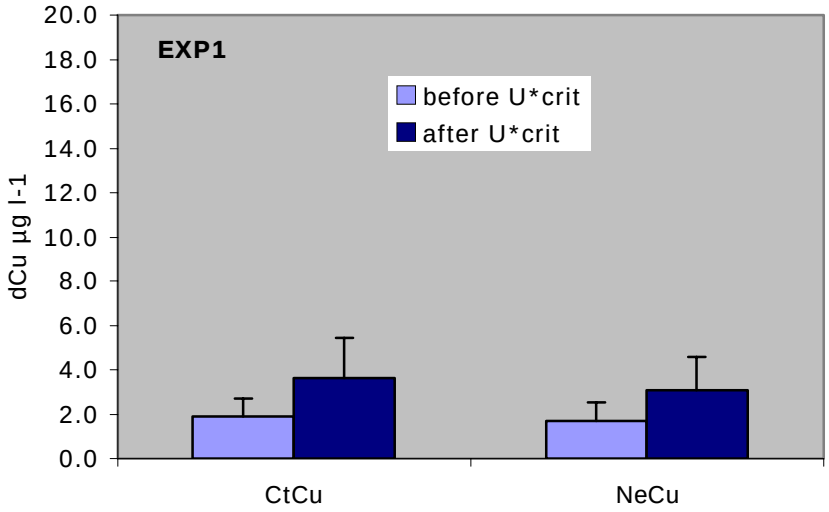

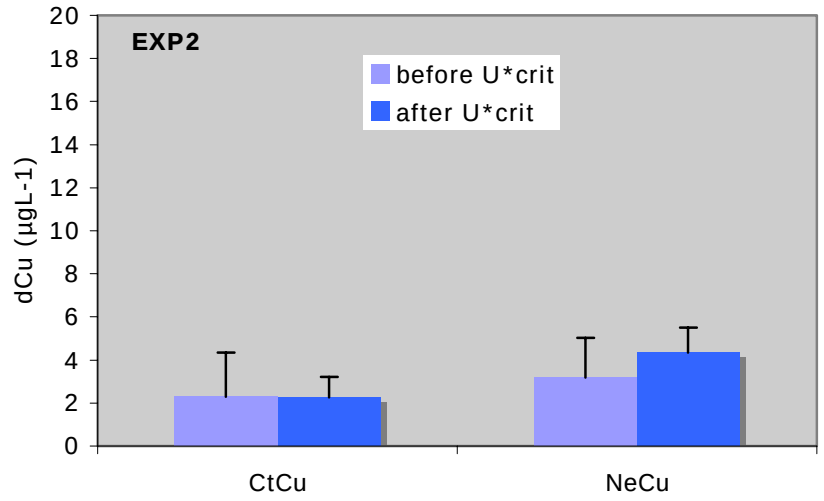

Figure 27 – Dissolved copper concentration (µg l^{-1}) before and after erosion (EXP1 – sediment contamination EXP2 - water-borne contamination).

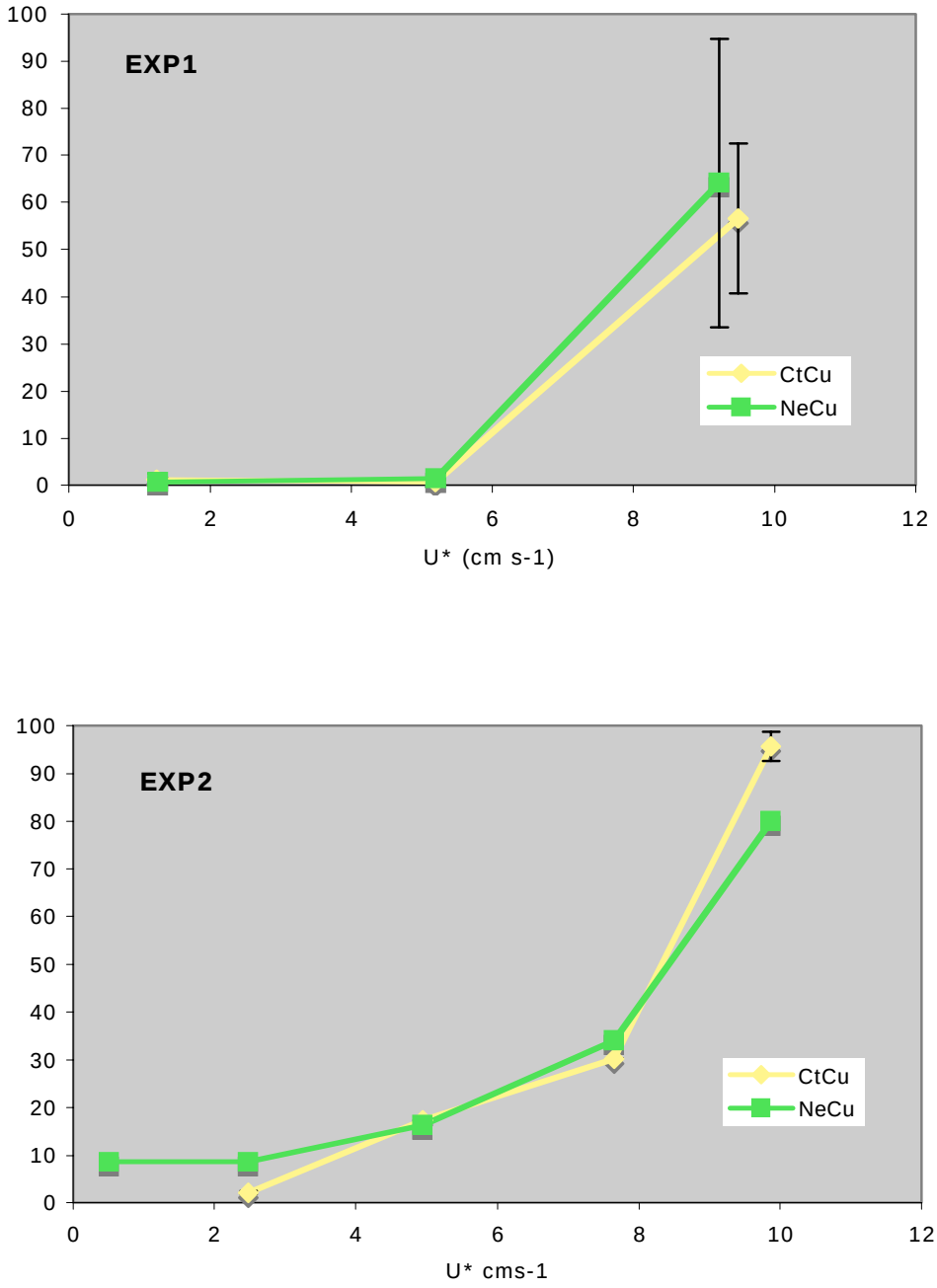

Figure 28 - Particulate copper concentration (µg l^{-1}) with increasing shear velocity (U* cms^{-1}) in the copper contaminated treatments in EXP1 (sediment contamination) and EXP2 (water-borne contamination).

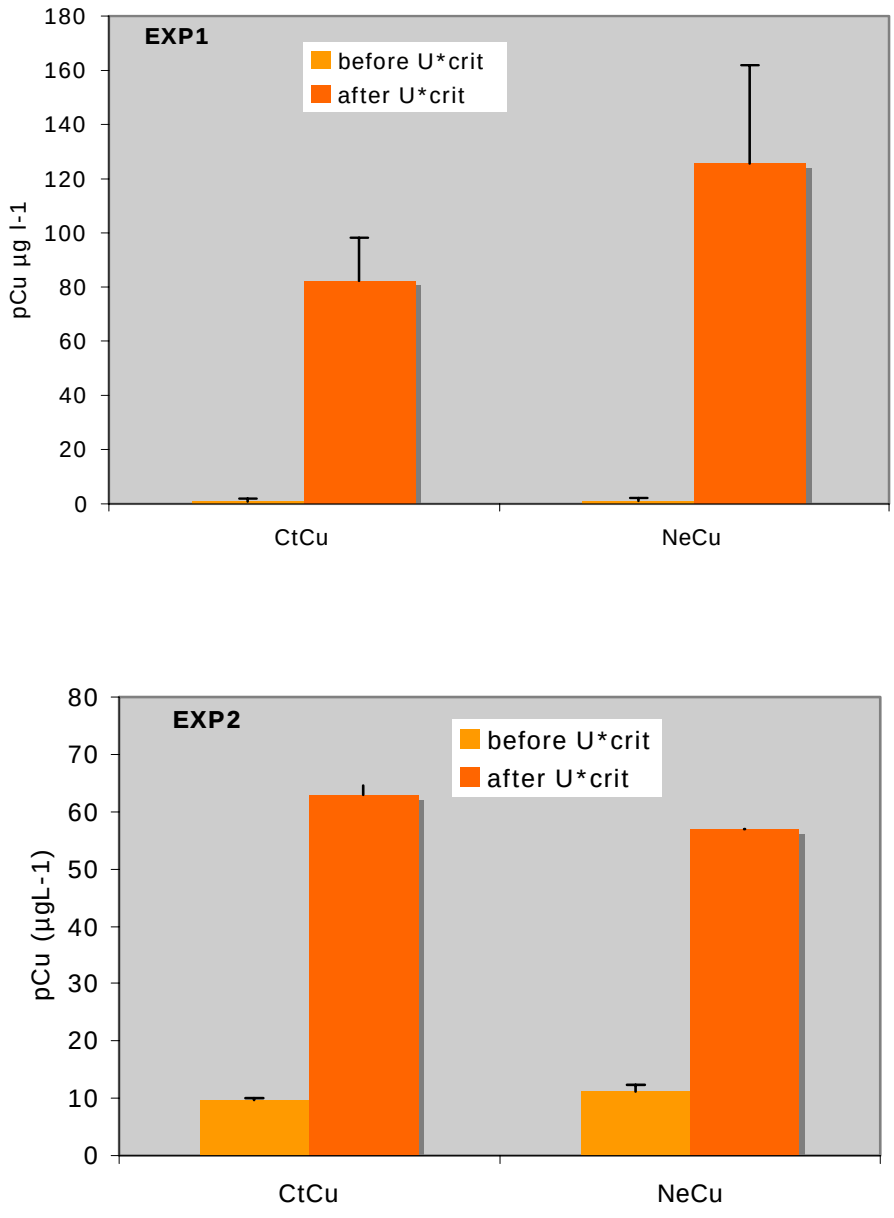

Figure 29 – Particulate copper concentration (µg l^{-1}) before and after erosion (EXP1 – sediment contamination EXP2 - water-borne contamination).

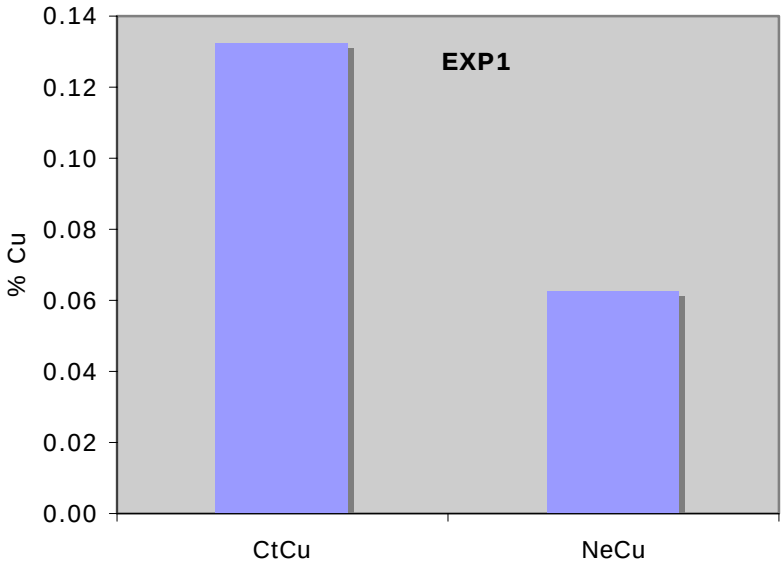

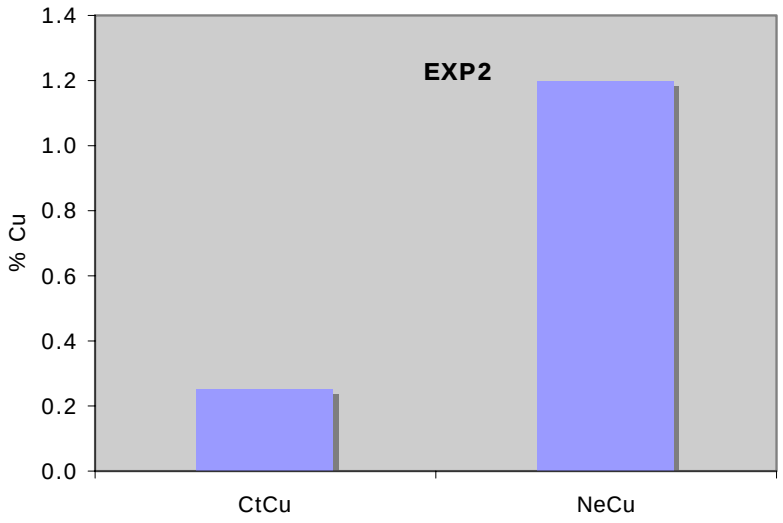

Figure 30 – Input of copper (%) from the sediment to the water column (as dissolved copper) after 20 min at U* 6.5 cms^{-1} (EXP1) and U* 4.1 cms^{-1} (EXP2).

Copper accumulation

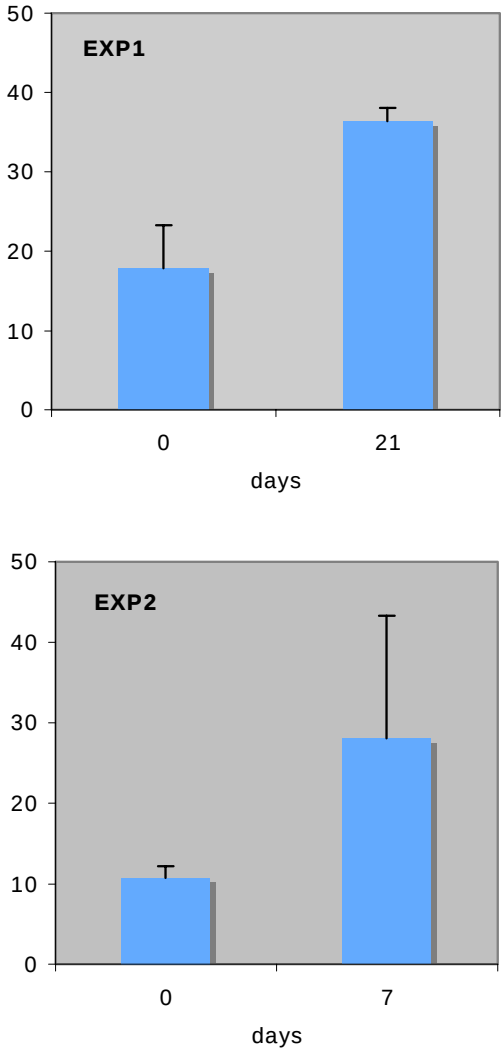

Figure 31– Copper content in the tissues of *N. diversicolor* after 21d exposure to sediment contamination (EXP1) and 7d exposure to water-borne copper contamination (EXP2).

Table 12 – Contamination conditions and accumulation of copper by *Nereis diversicolor*

	Manipulated sediment	Undisturbed sediment
Nominal contaminant concentration	200 mg Kg^{-1}	30 µg L^{-1}
Contamination mode	Sediment mixing	Water-borne
Exposure time (days)	21	7
Copper in the sediment (0-5mm, mg Kg^{-1})	167.03±2.3	45.86±21.9
Dissolved copper before erosion (dCu µg L^{-1})	1.7±0.8	3.2±1.8
Accumulation rate (µg Cu g^{-1} d^{-1})	0.86	17.28
Bioaccumulation factor (from dCu)	11	5
Mortality	-	25%

The use of two flumes with different hydrodynamic characteristics produced different erosion results. Annular flumes are known to have a compressed benthic boundary layer of just a few mm. This is a result of complex hydrodynamic conditions, namely secondary flows that increase shear velocity. The narrower the annular channel the better the approximation to a straight channel where hydrodynamic conditions are easier to determine.

Both flumes used in this project (a 15cm channel flume and a 10cm channel flume) were modelled (see the modelling section, page 56), considering a roughness factor of 2.5mm, in order to obtain a relationship between free-stream (U) and shear velocity (U*), that was then converted in shear stress (Pa). Shear velocity was ~25% of U for the 15cm flume and 10% of U for the 10cm flume.

Manipulated sediment erosion

Manipulated sediment erosion was initiated at high shear velocities indicating great cohesion of sediment particles (Fig. 21). A spongy layer (a 1mm biofilm) could be seen at the surface. This biofilm was responsible for the high resistance of the sediment to erosion. Once this layer was disrupted it would peel off and erosion started and progressed quickly.

The development of the biofilm was possible due to the stabilization of the sediment during 21 days under low continuous flow. This type of biofilm did not develop on the undisturbed sediments that were stabilized for 7 days only. These sediments eroded at lower shear velocities, as we will see later.

Sediment with added *N.diversicolor* showed a disturbed surface, no clear biofilm, higher erosion rates and higher eroded mass after 20 minutes at shear velocity of 7.7 to 8.7 cms-1, than did the sediment without *N.diversicolor*.

The contaminated sediment without *N.diversicolor* eroded more than its control.

Erosion depth varied between 0.6 and 1.3 mm, the highest being found in the presence of *N.diversicolor*.

Contamination may induce mortality and therefore less activity that generate carbohydrates that promote resistance to erosion. We know that the bioavailable copper was present in very low concentrations and so we could rather expect organisms to

produce more carbohydrates as a way of chelating copper and therefore reducing its toxic effects. This could mean more resistance to erosion when compared to non-contaminated sediments, which in fact was not observed.

No continuous monitoring of the suspended particulate matter with the stepwise increase in velocity was made in this experiment, and we could not clearly identify different erosion types (as in Amos, et al 1992). Nevertheless at higher velocities than the ones reported here, erosion rates in the contaminated sediments did not show a tendency to decrease with time and can be classified as Type II erosion. The other treatments showed Type I erosion (after an initial peak erosion rate decreased asymptotically with time). Shear stress was higher than what was observed by Amos et al 1992 for Type I erosion.

Burial and digging activities by *N.diversicolor* destroy the biofilm favouring erosion at lower shear velocities but enhance compaction of the subsurficial layers. The progression of erosion is related to the compaction of these layers. Although the four treatments showed the same shear strength at the surface (fall-cone) in the presence of *N.diversicolor* shear strength/compaction is higher. This means that although lower shear velocities are needed to start erosion, higher shear velocities than predicted by sediment alone will be needed to continue the eroding process.

Undisturbed sediment erosion

The undisturbed sediment behaved differently compared to the manipulated sediment. The 7 days period allowed for bioturbation and contamination to occur was not enough to develop a biofilm likely to peel off such as the one we had for the manipulated sediments.

There were also marked differences on the surface of the sediments with added N.diversicolor, as they appeared disturbed and powdery. The surface of both contaminated treatments had an orange-red colour and was clearly different from the controls.

A 10cm channel annular flume was used for the erosion runs with the undisturbed sediments and critical shear velocities (U*) were lower than the ones found for the manipulated sediments when using a 15cm channel flume. Differences in critical

erosion velocities may result from differences in the sediment properties and from differences in the hydrodynamic characteristics of the flumes.

Continuous monitoring of the suspended particulate matter with the stepwise increase in velocity was made in this experiment (Fig. 20). Erosion was Type I in the non-contaminated sediments and Type II in the contaminated sediments. Shear stress at 40cms-1 was 1.7 Pa, below the values found by Amos et al 1992, for Type II erosion. We must bear in mind that calculated shear stress takes into account a roughness of 2.5mm, a value that is likely to be underestimated in the case *N.diversicolor* is present.

Contaminated sediments with and without *N.diversicolor* eroded at lower critical shear velocities(U*) than the non-contaminated treatments (Fig. 21), resulting in higher eroded mass at 40cms-1 (U* 4cms-1). Eroded mass was particularly high in the contaminated sediment without *N.diversicolor*. This is in agreement with the fact that erosion of the subsurficial layers when galleries are present occurs at higher shear stresses that what would be predictable.

Erosion depth varied between 0.6 and 2.6 mm (the highest value was registered in the contaminated control)

Eroded chlorophyll *a* does not match the surface content of this pigment for the four treatments, where surprinsingly high values were found in the contaminated control. Eroded Chla was high in the control and the 3 other treatments had lower values, as expected. Eroded pheopigments are higher in the contaminated sediments, in result of toxicity and degradation. *N.diversicolor* reduces chlorophyll *a* in the sediment surface and therefore reduces the content eroded (Fig. 22).

Because at the same time it destabilizes the surface, it increases eroded mass and therefore also increases the amount of chlorophyll *a* that is eroded to the water column.

Eroded Chla in the water can reach up to 50% of the surface chlorophyll *a* and eroded pheopigments can reach up to 69% (Fig. 23).

Eroded carbohydrates are not related to surface contents. The control sediment showed the lowest contents so that the concentrations eroded in the treatment must come from layers below 5mm. Though this might have happened punctually we suspect that the carbohydrate contents in the surface sediment are underestimated. Eroded EPS-S is lower in the contaminated sediment sustaining the hypothesis of algal cell mortality due to toxicity. Eroded EPS-EDTA on the contrary are higher in the contaminated sediment in relation to mucus secretion by the biota to avoid toxicity (Figs 24 and 25).

Mortality occurred in the contaminated sediment and decomposition by bacteria may have contributed to increase the EPS-EDTA fraction.

No relation was found between EPS-S content in the 0-5mm before erosion and sediment stability (as U*crit), but a negative relation exists between eroded EPS-S and U*crit, confirming the stabilizing nature of the EPS.

Erosion is a major process for input of materials to the water column. From Table 13 we can conclude that bioturbation is very important in facilitating coupling of benthic and pelagic processes, making available organic materials for pelagic organisms.

3.1.3. Summary of the effects of bioturbation and contamination on the input of materials to the water column

Inputs of materials to the water column were calculated as % of the surface sediment content of that material. Multiplying factors for the effects of bioturbation, contamination and both combined and are summarized in Table 12.

In manipulated sediments bioturbation increases SPM 2.5 times at shear velocities ~4cms^{-1}; with contamination the effect increases SPM 1.5 times

In undisturbed sediments bioturbation increases SPM twice at shear velocities ~4cms^{-1}; with contamination the effect is not relevant at U* 4cms^{-1}, but higher velocities (~6cms^{-1}) SPM increases 3 times

Copper input was always below 1.2% and mostly <0.5%; bioturbation effects on copper input range from 0.5 to 4

Chlorophyll a input ranges from 11- 51% and bioturbation duplicates this input

Pheopigments input ranges from 7 – 69% and contamination increases input 5 to 10 times)

EPS-S input ranges from 34 -~100% (contamination reduces input by 10-70%)

EPS-EDTA input ranges from 14- ~100% (bioturbation increases input 4.5 times)

Table 13 – Factors for bioturbation, contamination and both combined effects on the **input of materials** to the water column for shear velocities of ~4 cms^{-1}. (italics - manipulated sediments; Cu – contaminated sediments; N – bioturbation by *N.diversicolor*)

Materials	Bioturbation effect	Contamination effect	Combined effects
SPM	2 – *2.7* 1.5* - *1.5*	*1.5* – 6 *0.8* – 2 (N)	*2.2* - 4
Copper	*0.5* - 4	-	-
Chlorophyll a	1.5 2 (Cu)	2 0.5 (N)	0.7
Pheopigments	0.7 2 (Cu)	2 10 (N)	6
EPS-S	0.2 1.5 (Cu)	<0.1 0.7 (N)	0.2
EPS-EDTA	<0.1 2.2 (Cu)	0.2 4.5 (N)	0.4

*shear velocity ~6 cms^{-1}

3.2. Modelling applications and results

3.2.1. Annular flume model simulations setup

Due to the small spatial scales of the flume, Coriolis force is neglected and water density is considered to be constant, assuming only barotropic flow.
In the performed simulations, the k-ε model included in GOTM, for calculating vertical turbulent eddy viscosity, was used. This model consists in solving a transport equation for turbulent kinetic energy (k) and turbulent kinetic energy dissipation (ε). Horizontal eddy viscosity was considered constant, after some calibrations, in the order of 10^{-4} m^2/s.

Geometry parameters are given as input data to the model. This means that the dimensions of the annular flume can be different in different simulations, just by introducing a different geometry parameters file. Nevertheless, all the simulations performed to test the model were applied with the dimensions of the annular flume operated in the laboratory (

Table 1).

Table 14 - Annular flume geometry parameters

Water column height	32.5 cm
Exterior diameter	60 cm
Interior diameter	40 cm
Channel width	10 cm

Various discretizations were used, combining fine resolution with time step, having in mind the type of flow generated in this kind of domain. A final horizontal discretization of 20x72 cells was used (Figure), with 40 layers vertical discretization using a sigma coordinate type, with a non-constant spacing (Figure 3).

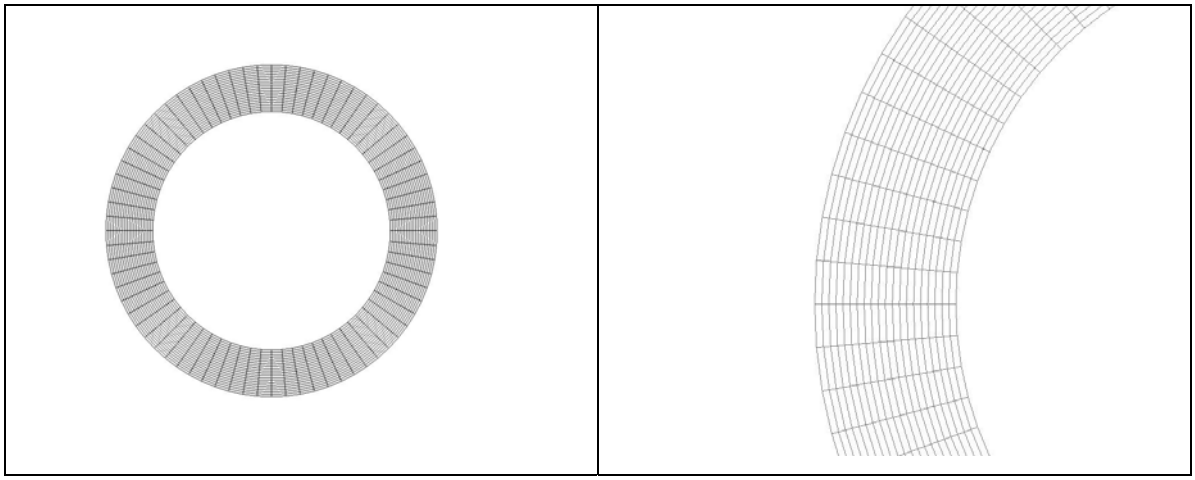

Figure 32 - Horizontal grid discretization

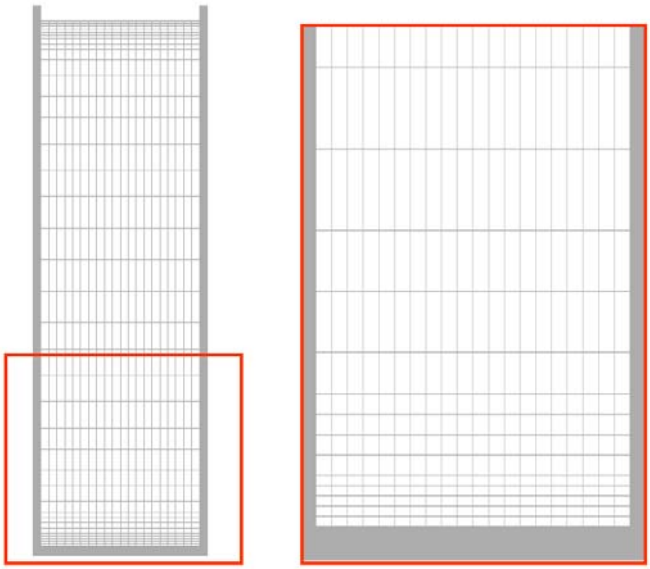

Figure 33 – Transversal cut of the annular flume. Detail of vertical discretization near the bottom.

Hydrodynamics solution is forced by applying a shear stress directly at the surface of the water column. This approach is made, in order to simulate the actual mechanism that forces water to flow in the annular flume operated in the lab, as MOHID does not support complex geometries in surface boundary conditions, such as the plate used in the laboratory. Therefore, some limitations are expected in the validation of the model. This surface forcing provides momentum to the upper layer of the water column that by turbulent diffusion is transported to the lower layers and enables the water to speed up.

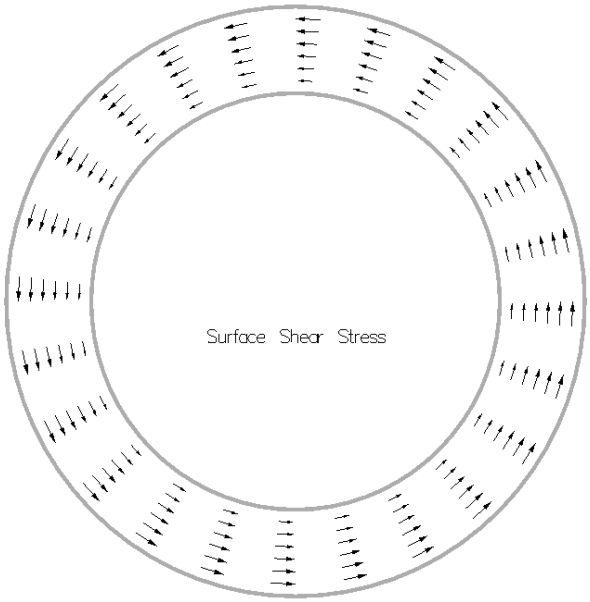

Figure 34 – Example of imposed shear stress at the surface boundary (vectors plotted every 3 cells)

The shear stress is imposed as constant, enabling steady state flow conditions to develop. Shear stress vectorial field is previously rotated to the Cartesian plane (Figure).

A non-slipping condition was considered to both the bottom and lateral boundaries, having the latter the most important contribution to the shear forces. Cyclic boundary conditions are considered, to assure continuous flow, both in the hydrodynamic module and in mass transport model.

2.2.2. Hydrodynamics

ADV measurements and bottom boundary layer characteristics

Laboratory data measurements were performed in the annular channel using an ADV currentmeter (Sontek® Micro-ADV).

Four scenarios were set up for performing measurements, namely through applying four different rotation velocities to the channel plate, representing four (assumed) stabilized flow fields.

Each velocity scenario was defined by measuring approximate velocities of 5, 10, 20 and 40 cm/s at 10 cm above the bottom of the channel, after 5 minutes stabilization. Velocities were measured in the centre of a flume section (width = 10 cm) along the vertical axis from the bottom of the channel till 10 cm above.

The profile points were chosen in order to present a denser distribution near the bottom, where gradients are higher, so that a better discretization was observed.

Figure presents the near-bottom velocity profiles for the 4 designed scenarios, in the rotation axis, therefore representing the main component of the flow field.

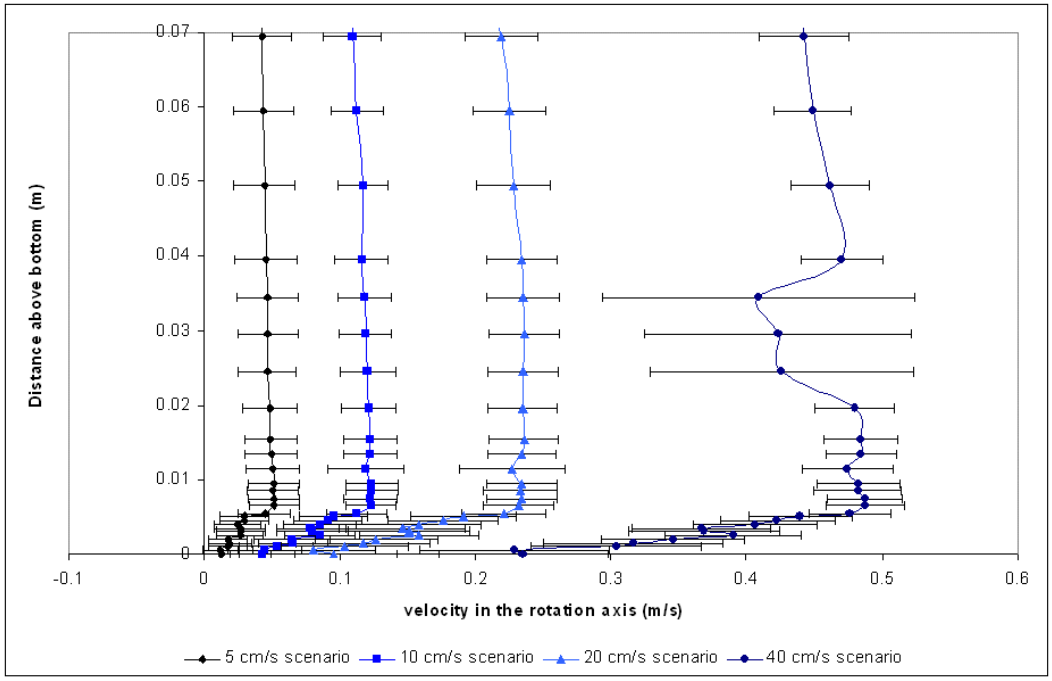

Figure 35 - Rotation axis velocity profiles for the 4 scenarios

It is visible that for all scenarios the boundary layer is compressed to about 5-6 mm, which might be the result of the presence of secondary flows, as it can be seen in Figure

.

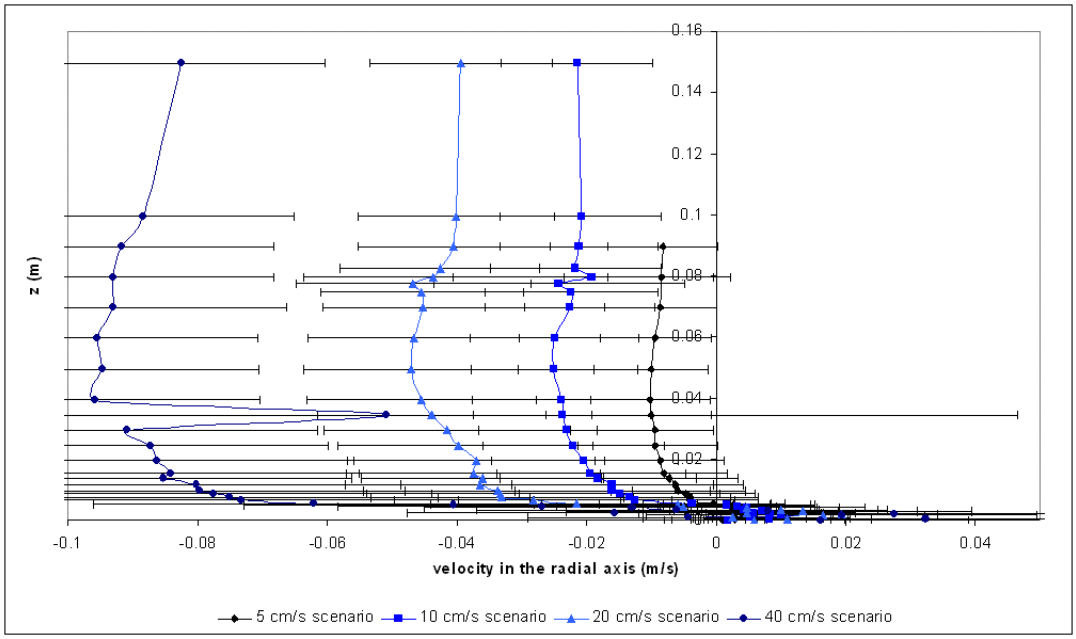

Figure 36 - Radial axis velocity profiles for the 4 scenarios

Modelling results and validation

Simulations were performed reproducing the scenarios drawn in the ADV measurements. A validation of model results is perform by comparing measured and modelled velocity profiles in the rotation, radial and vertical axis. Results for the 40cm/s scenario are not presented here has a stable velocity field was not possible to obtain, due to the method used to simulate and impose surface boundary conditions, which for that range of velocities, it is probable to cannot be assumed.

Rotation axis velocity profiles

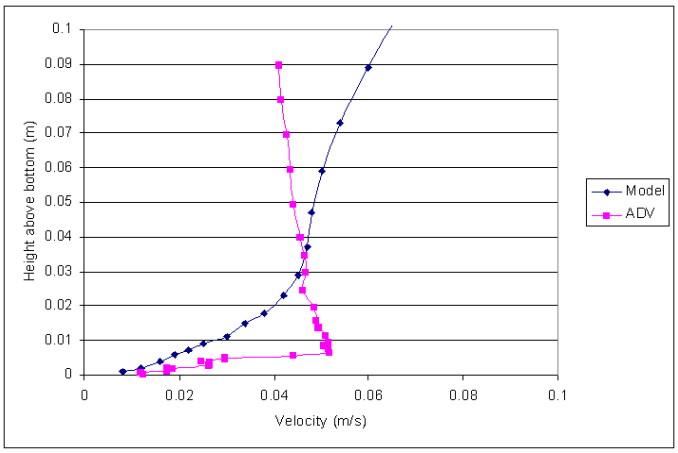

Figure 37 - Comparison between model and ADV rotation axis velocities for the 5cm/s scenario

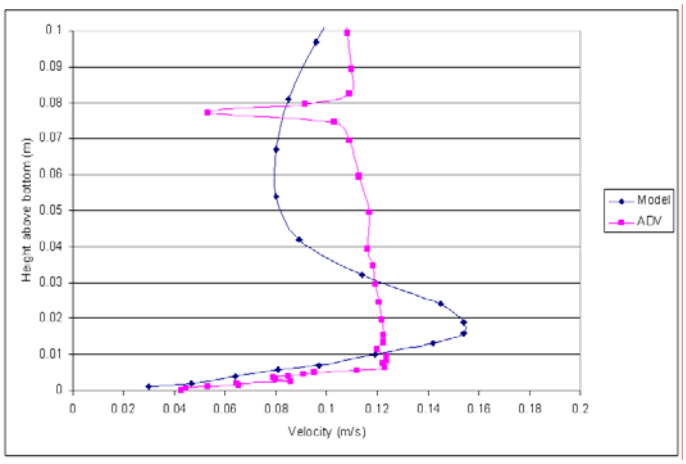

Figure 38 - Comparison between model and ADV rotation axis velocities for the 10cm/s scenario

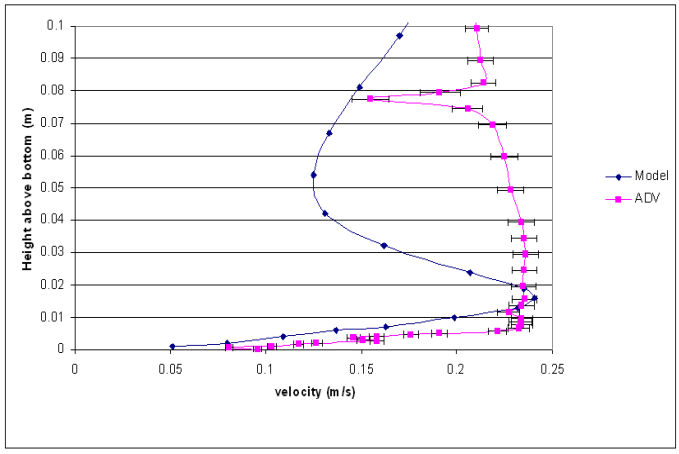

Figure 39 - Comparison between model and ADV rotation axis velocities for the 20cm/s scenario

Radial axis velocity profiles

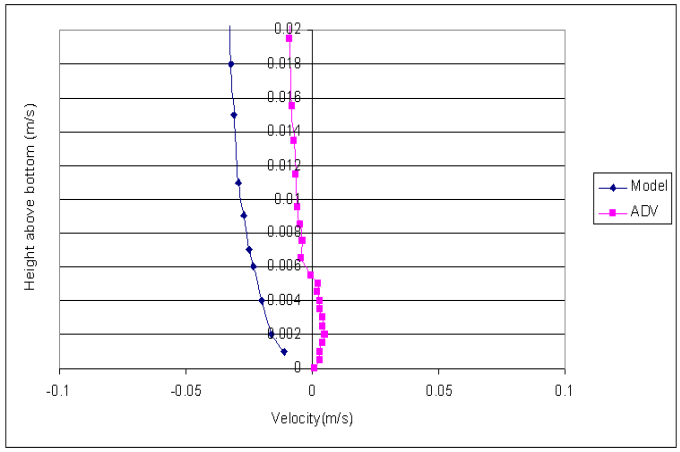

Figure 40 - Comparison between model and ADV radial axis velocities for the 5cm/s scenario

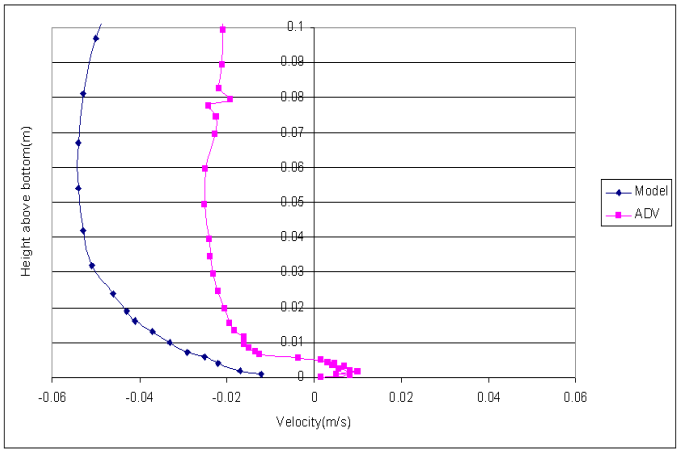

Figure 41 - Comparison between model and ADV radial axis velocities for the 10cm/s scenario

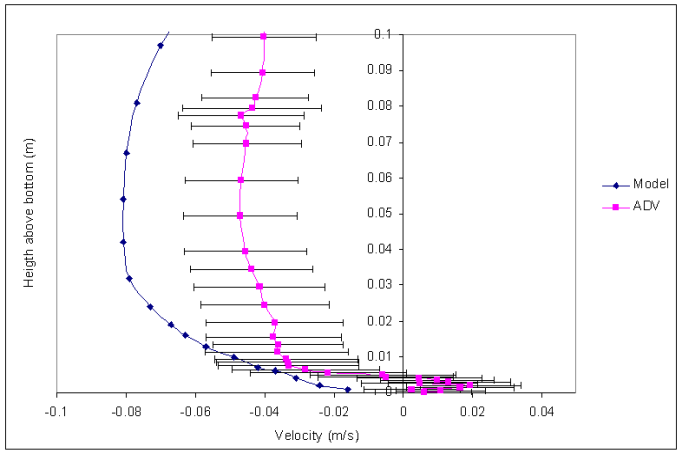

Figure 42 - Comparison between model and ADV radial axis velocities for the 20cm/s scenario

Vertical axis velocities

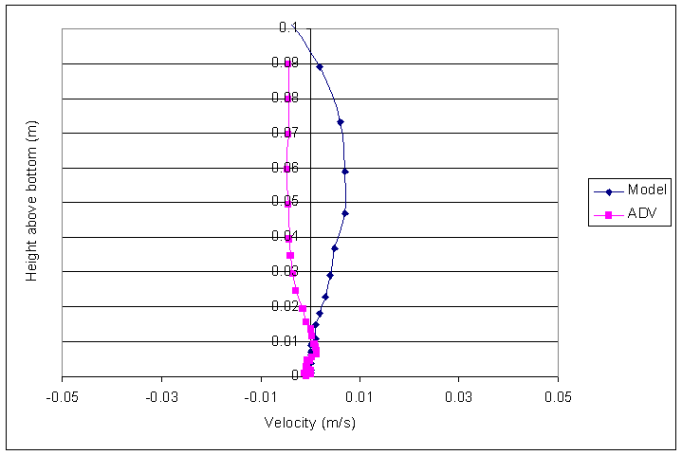

Figure 43 - Comparison between model and ADV vertical axis velocities for the 5cm/s scenario

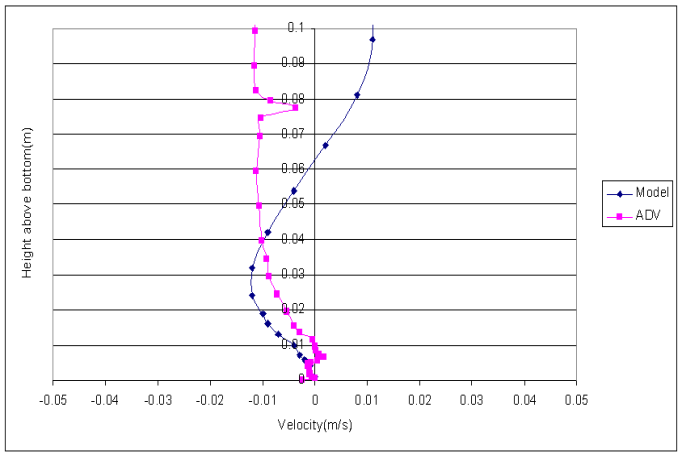

Figure 44 - Comparison between model and ADV vertical axis velocities for the 10cm/s scenario

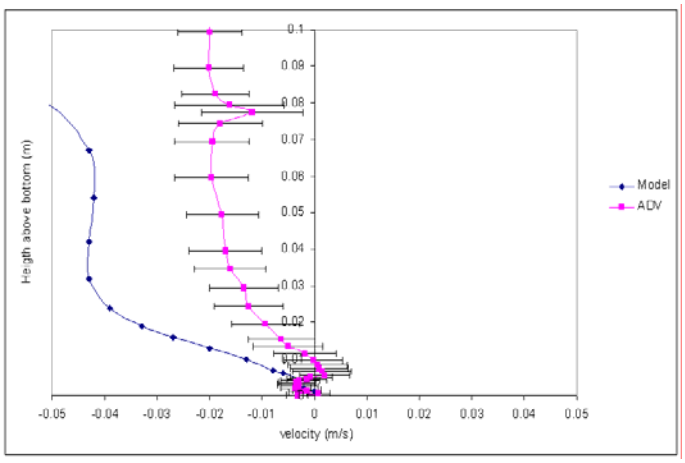

Figure 45 - Comparison between model and ADV vertical axis velocities for the 20cm/s scenario

Results show a relatively satisfactory agreement in terms of secondary flow orientation, and a satisfactory pattern of velocity intensity. Therefore, one can assume, given the limitations of the model, that the overall annular flume flow pattern is solved, with a good approximation of the bottom boundary layer characteristics.

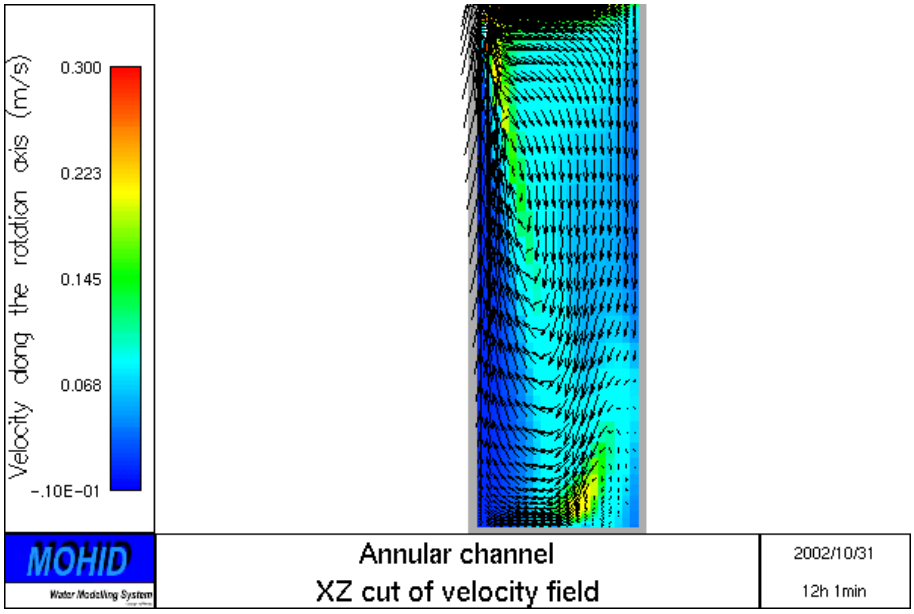

Figure 46 – Aspect of the velocity field in a radial cut - 10cm/s scenario

Bottom shear stress

A variety of models can be applied to derive bottom shear stress from the mean flow velocity. In a turbulent flow, such as in the annular flume, the bottom shear stress (τ_b) is normally defined by a quadratic relation with the shear velocity u_*.

$$\tau_b = \rho u_*^2$$

where ρ is the water density. Several descriptions can be found in literature to define shear velocity, normally based in empirical expressions related with parameters such as rugosity (type of bottom), gravity, and water column height. A well accepted calculation is the log-law of the wall, presented in the model description.

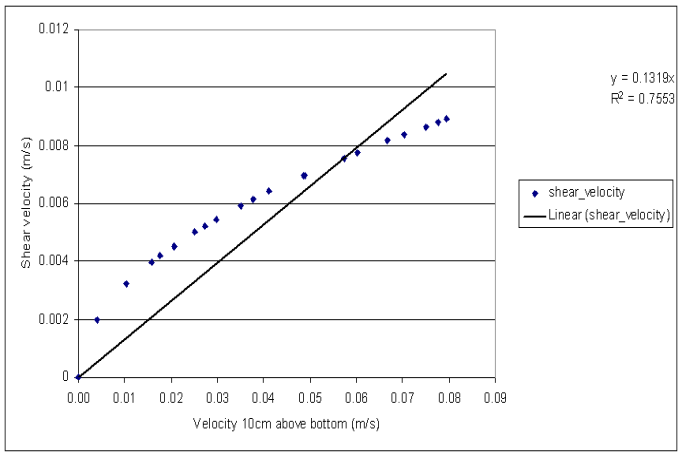

Figure 47 – Shear velocity vs velocity 10 cm above bottom – 5cm/s scenario

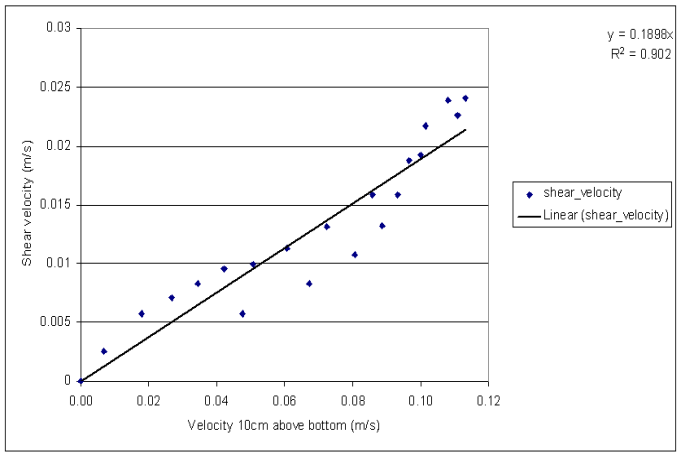

Figure 48 – Shear velocity vs velocity 10 cm above bottom – 10cm/s scenario

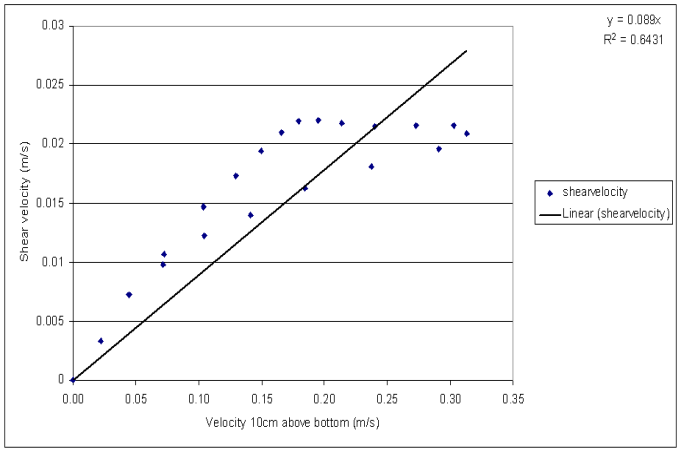

Figure 49– Shear velocity vs velocity 10 cm above bottom – 20cm/s scenario

Shear velocities computed by the model were plotted against velocities 10cm/s above the bottom (i.e. scenario velocity) for a radial section of the flume. Relation between the two variables varies from $u_*=0.1319u$ for the 5cm/s scenario, $u_*=0.1898u$ for the 10cm/s scenario and finally, $u_*=0.089u$ for the 20cm/s scenario. No clear relation can be found, but an order of magnitude of 0.1-0.15 u_* /u, can be considered as a fair approximation for the 10cm width flume.

3.2.3. Sediment transport

Bottom shear stress is recognisably a governing factor in sediment transport processes, as it controls erosion and deposition, therefore regulating the distribution of sediments between the bed and the water column. As seen above, the flow patterns in the annular flume are complex, due to the differential distribution of the velocity fields in the rotation axis and due to the presence of pronounced secondary flows across the channel. This will have an important contribution on the bottom shear stress distribution, and ultimately on creating differential sediment erosion zones.

Testing new model developments

Erosion and deposition processes were already implemented into the model, but were only applied at the sediment water interface to recent deposits. This meant that when the superficial sediment layer was totally eroded, erosion stopped. However, as described before, depth dependent differential erosion rates were included and the new algorithm for the sediment vertical coordinate needed to be tested. This is one of the key processes

implemented in the model, as it is enabled to collapse control volumes, allowing to compute the vertical sediment column with a variable number of layers during run-time. In the "empty" layers, sediment and interstitial water volumes are set to zero, as well as properties concentrations. This is accomplished, as defined in the model description, by a mass conserving algorithm that attaches and detaches two layers as minimum and maximum thicknesses are reached.

In order to test this feature, an idealized model was setup in order to obtain bottom shear stress higher than critical shear stresses for erosion until a certain depth.

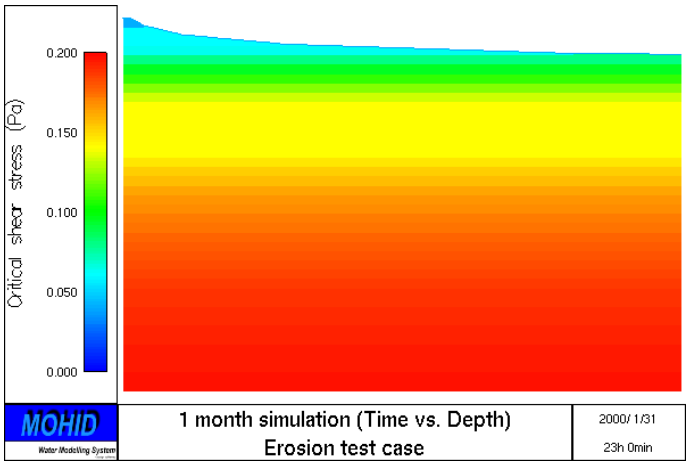

Figure 5 - Top layers collapsing in erosion test case

Results are purely illustrative of the way top sediment layers collapse as they reach minimum thickness allowed, in this case 1mm (Figure).

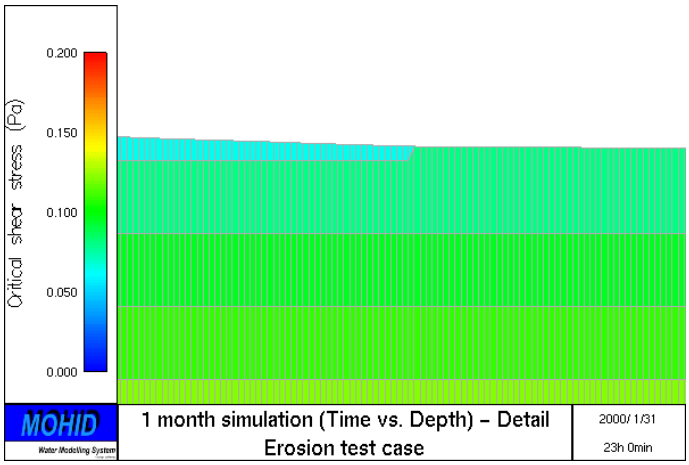

Figure 51 - Detail of collapsing layer in erosion test case

Also, as described before, erosion occurring from the sediment compartment results in a flux of interstitial water to the water column. With this flux, solutes present in interstitial water are also flushed to the water column. A simple test case is presented, in which the sediment interstitial water was initialized with constant conservative tracer concentration (1 mg/l) and the water column with null tracer concentration and null SPM concentration. Porosity in the sediment was considered 0.5. Thus for each sediment control volume, half is water and the other half is dry sediment. This way in terms of the control volume and considering sediment dry density equal to 2300 kg_{sed}/m^3sed, the "concentration" ratio between sediment and the dissolved tracer will be $2.3x10^6$, being this ratio maintained in the water column as erosion takes place (Figure).

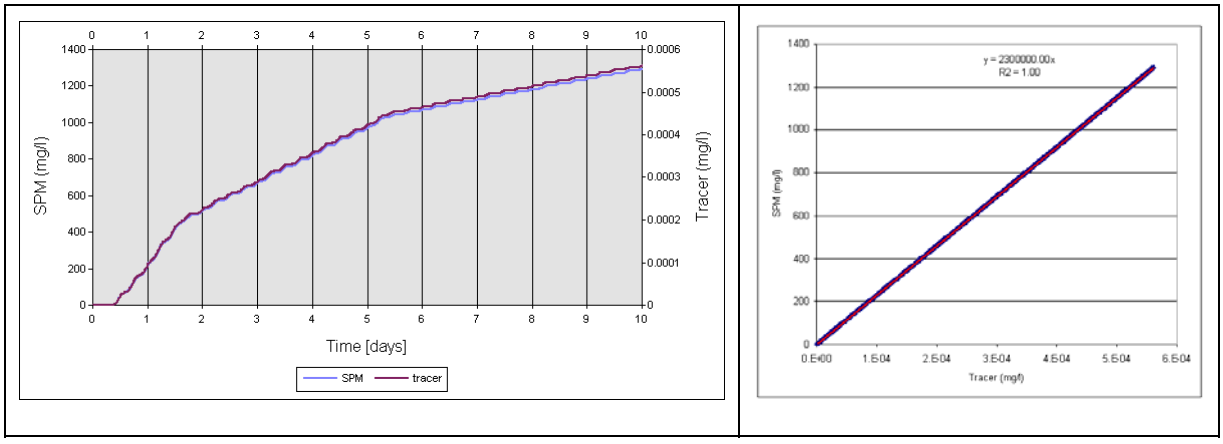

Figure 52 - Erosion of a tracer dissolved in interstitial water. SPM and tracer concentrations in the water column (on the left) and ratio between them (on the right).

Simulations in the annular flume

Although model results cannot reproduce entirely the flow patterns in the annular flume, due to the limitations described above, it has been shown that it is able to compute acceptably the boundary layer characteristics which results in a good approach of bottom shear stress that controls sediment transport processes such as erosion or deposition.

Therefore, it is possible to assume that the major hydrodynamic processes in the annular flume can be modelled and that a sediment transport model can be coupled to the 3D hydrodynamic model and applied in order to reproduce laboratorial experimental work.

A simulation was setup for the 20cm/s scenario, which as seen, results in shear velocities around 2cm/s and shear stress of around 0.4Pa. This was the critical shear stress for measured for the undisturbed sediment with influence of bioturbation and contaminated with copper, which after 20 minutes of erosion resulted in SPM concentrations in the water column, in the order of 500mg/l.

The sediment compartment was defined with 100 layers relative to 5cm thickness, with critical shear stress increasing exponentially with depth.

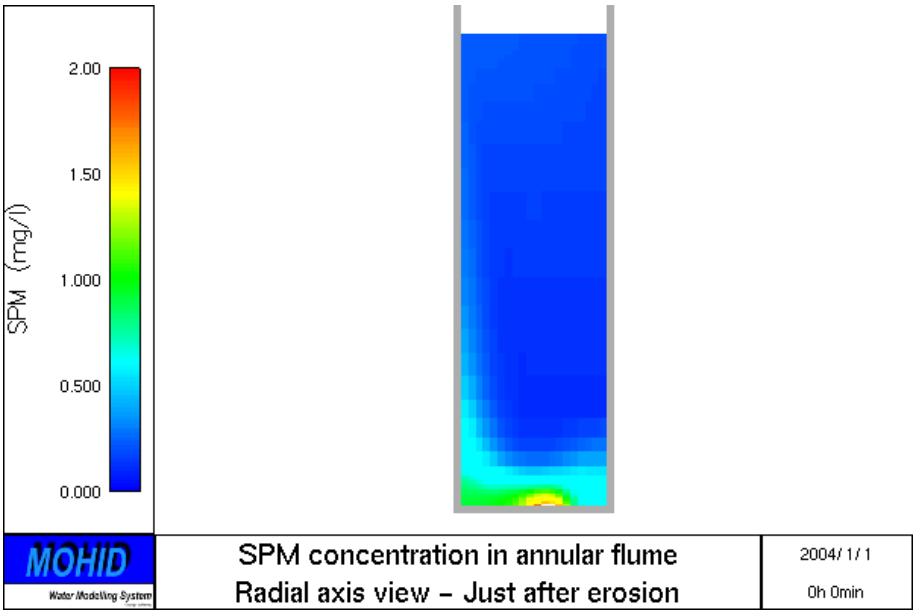

Figure 53 – SPM distribution just after erosion occurs

Figure 53 presents a radial axis view of the flume, a few seconds after the erosion critical shear stress has been exceed and resuspension occurs.

Concentrations after 20 minutes can be observed in figure 54, where reaching up to 250 mg/l, with near-bed concentrations up to 1000mg/l.

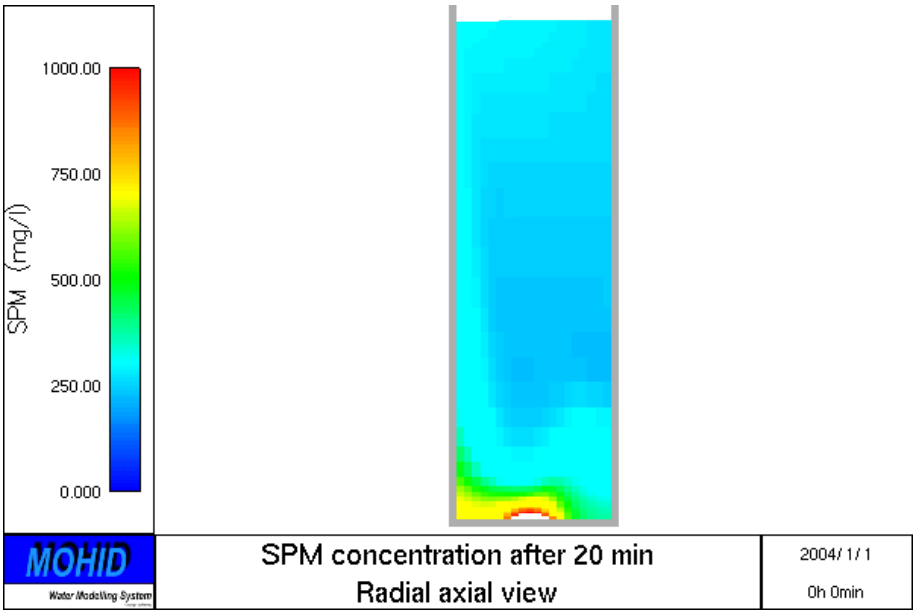

Figure 54 – SPM concentrations after 20min

4. Considerations and concluding remarks

4.1. Laboratory experiments

Manipulated or undisturbed sediment?

Due to the large differences in the way manipulated and undisturbed sediments behaved regarding erosion, we feel that manipulating the sediment leads to deviations from reality and should be avoided. We may speculate that manipulated sediments are "more equal" among them and that the obtained results are more directly related to the differences imposed among treatments, (all else being equal). But it does not represent field conditions.

In our case the flume is small and it is fairly easy to collect undisturbed sediment. The question arises when using large flumes with large working sections, it might be impossible to collect undisturbed sediments.

Using the whole bottom of the flume instead as a work section is also more correct. It behaves as a continuous working section with no edges and no scouring occurs.

Working with undisturbed sediments means working with natural patchiness of biogeochemical properties and so more than 3 replicates are needed.

The contamination of the sediment as a whole poses another problem, as this is only possible by mixing, i.e. manipulating, the sediment.

Contaminating the sediment with a water-borne contaminant is not effective, only the surface is in close contact with the contaminant that does not penetrate the sediment. In our case contaminating the water also imposes higher toxicity on the animals and cause mortality, which to a certain extent limits its use (if we are analysing the effects of bioturbation we want the animals to be active).

Using natural contaminated sediments seems to us to be the best option, but in our case it was not possible to find such sediments at the sites available. (These sites have to be of easy access by car, with more or less compact mud and relatively safe to walk on).

To improve the methodology we recommend:

- The use of undisturbed sediments

- The use of two flumes simultaneously, one for sediment properties after stabilization and before erosion, the other for erosion runs and inputs to the water column
- Taking ADV measurements simultaneously with erosion runs to assess the modification of shear stress at different velocities and characterize the hydrodynamics of the benthic boundary layer

Input of contaminants to the water column

The input of contaminants from the sediments to the water is related to sediment mobility. The ability of sediments to retain these compounds (chelating and adsorption processes) makes them well-known contaminant sinks. Mobilizing sediment, for instance while dredging, is probably an important route of input of contaminants to the water column. With the increase of suspended contaminated particles of sediment the probability of contaminants passing to the dissolved phase, the most toxic towards the biota, also increases.

High copper concentrations were found adsorbed to particles in suspension. According to size, these particles can be ingested and copper made available to filter feeding animals (i.e. dissolved copper) in the digestive tract, but this was not investigated in this project.

We found that in general less than 0.5% of the copper present in the sediment passes to water as dissolved copper.

N.diversicolor as bioturbator: surface *vs* deeper layers

Bioturbation by *N.diversicolor* has profound effects on sediment erosion. N.diversicolor is a surface destabilizer, and promotes erosion at lower shear velocities. However, above U*~4cms^{-1} the shear stress needed to continue eroding the subsurficial layers, when galleries are present, is higher than would be expected, This originates lower suspended matter inputs with *N.diversicolor* than without, for the same shear velocities

Higher current velocities are therefore needed to erode deeper layers, where compaction is higher and cemented complex galleries occur. Scouring at the galleries openings

increases bed roughness, (which was not measured but should be higher in the presence of N.diversicolor and increase as erosion progresses), which increases shear stress and adds to the factors that promote erosion.
As stated before, compaction of deeper layers of the sediment maybe an experimental artefact imposed by animal density and the physical limitation of the walls and bottom of the flume. More research will be needed to investigate density dependent effects on sediment properties and what happens in field conditions.

4.2. Modelling

MOHID Water Modelling System is prepared to simulate water flow and cohesive sediment transport in an annular flume, therefore presenting to be an important numerical tool in this kind of studies, and particularly in the framework of this project and future research projects.

Simulations results were found satisfactory as one must understand the complex flow occurring in the annular channel, and by the fact that data measured with the ADV is not completely representative of the flow, as profiles were taken in only one point of the channel section (due to practical reasons, the ADV is fixed to the flume and can only be moved along the vertical axis).

Although modelling results could not reproduce entirely the measured flow patterns in the annular flume, due to the limitations described above, such as the complexity of the surface boundary condition and the assumption of the hydrostatic hypothesis, it has been shown that it is able to compute acceptably the boundary layer characteristics, a governing factor of sediment transport processes, namely erosion and deposition.
Therefore, it is possible to accept that the major hydrodynamic processes in the annular flume were reproduced and that the sediment transport model could be applied, in order to reproduce laboratorial experimental work in a straightforward way.

MOHID, was originally designed as a coastal and estuarine hydrodynamic model, and has been applied successfully to a large number of coastal, estuarine and oceanic systems. It has also been generalized, applied and validated in water reservoirs simulations, what reinforces its robustness and versatility. The limits of applicability were once more tested in this project and with satisfactory results, showing that the

model presents itself as a powerful scientific tool, and opening perspectives for improvements in cohesive sediment transport modelling and on the coupling of biological and physical process.

New discretizations and new processes were added to the model, adding versatility and knowledge to the model, which is now ready to be tested and applied to real systems. The new developments created in the framework of this project are ready to increase reliability in the model and to improve the understanding of sediment and contaminant transport processes.

5. Further investigation

Interesting aspects resulting from this project that need further investigation are

⇒ Density dependent effects of macrofauna (namely *N.diversicolor*) on sediment properties and erosion processes

⇒ Comparing the effects of bioturbation by N.diversicolor with other functional groups, such as bivalves, crabs.

⇒ Interactions between the hydrodynamics of the benthic boundary layer and bioturbation, (structures as protruding shells and siphons, and exhalent jets. Epifaunal and endofaunal siphonate and non.siphonate bivalves should be considered.

⇒ Validating laboratory results in the field

⇒ Testing the improved model for sediment transport in field conditions

6. References

Backhaus, J. O. and Hainbucher, D., 1987. A finite-difference general circulation model for shelf seas and its application to low frequency variability on the North European Shelf. In: J. C. J. Nihoul and B. M. Jamart (eds.), Three-Dimensional Models of Marine and Estuarine Dynamics, Elsevier Oceanography Series, 45: 221- 244

Boudreau, B.P., 1996, The diffusive tortuosity of fine-grained unlithified sediments. Geochimica et Cosmochimica Acta, 60, 3139-3142

Boudreau, B.P., 1997, A one dimensional model for bed-boundary layer particle exchange, Journal of Marine Systems, 11, 3-4, 279-303

Braunschweig, F., P. Chambel, L. Fernandes, P. Pina, R. Neves, 2004, The object-oriented design of the integrated modelling system Mohid, Computational Methods in Water Resources International Conference, Chapel Hill, North Carolina, USA

Flemming B. W. and Delafontaine M. T. 2000.Mass physical properties of muddy intertidal sediments: some applications, misapplications and non-applications
Continental Shelf Research, Volume 20, Issues 10-11:1179-1197

Hans Burchard, Karsten Bolding, and Manuel Ruiz Villarreal - GOTM - a general ocean turbulence model. Theory, applications and test cases. Technical Report EUR 18745 EN, European Commission, 1999.

Hayter, E. J., C.V. Pakala, 1989, Transport of inorganic contaminants in estuarial waters, Journal of Coastal Research, Special Issue 5, 217-230

J. Smagorinsky, General circulation experiments with the primitive equations, Monthly Weather, Review, 91(3), (1963), 99–165.

Krone, R., 1962, Flume Studies of the Transport in Estuaries Shoaling Processes, Hydr. Eng. Lab., University of Berkeley, California, USA

Leendertse, J. J. and Liu, S. K., 1978: A Three-dimensional turbulent energy model for non-homogeneous estuaries and coastal sea systems. Hydrodynamics of Estuaries and Fjords, J.C.J. Nihoul Ed., Elsevier Publ. Co., Amsterdam, pp. 387-405.

Mehta, A. J., 1988, Laboratory Studies on Cohesive Sediment Deposition and Erosion, Physical Processes in Estuaries, Springer-Verlag, Berlin Heidelberg New York, Job Dronkers and Wim van Leussen (Editors)

Mellor, G. L. and Yamada, T., 1982: Development of a turbulence closure model for geophysical fluid problems. *Rev. Geophys. Space Phys.*, **20**, 851-875.

Nihoul, J.C.J., A three-dimensional general marine circulation model in a remote sensing perspective, In Annales Geophysicae, 2, 4, 433-442, 1984

Pacanowski, R. C. and G. H. Philander, Parameterization of vertical mixing in numerical models of tropical oceans. J. Phys. Oceanogr., 11, 1443-1451, 1981

Partheniades, E., 1965, Erosion and Deposition of Cohesive Soils, J. Hydr. Div., ASCE, 91 (1), 105-139

Pina, P., 2001, Integrated Approach to Study the Tagus Estuary Water Quality, Dissertação para a obtenção do grau de Mestre em Ecologia, Gestão e Modelação de Recursos Marinhos, Instituto Superior Técnico, Lisboa

UNESCO, 1981, Tenth Report on the joint panel on oceanographic tables and standards, Technical papers in marine science, N. 36, 24 pp

Yang, Z., Baptista, A. and Darland, J. - Numerical modelling of flow characteristics in a rotating annular flume. Dynamics of Atmospheres and Oceans, 31, pp. 271-294, 2000.

7. Publications resulting from this project

Thesis

"Modelling of arsenic dynamics in the Tagus estuary", MSc Thesis in Ecology, Management and Modelling of Marine Resources, Instituto Superior Técnico, Technical University of Lisbon, 2005

International journals

"Erosion of cohesive undisturbed sediments: effects of copper contamination and bioturbation by *Nereis diversicolor* on the input of materials to the water column." Sobral P. and Figueiredo S. (in preparation)

"Hydrodynamic and sediment transport modelling in an annular flume: the effects of bioturbation on erosion processes", Fernandes, L., Leitão, P.C., Sobral P., Fernandes, S., Neves, R. (in preparation)

"Erosion thresholds and biogeochemical properties of undisturbed cohesive sediments after bioturbation by *Nereis diversicolor"* P. Sobral & S. Figueiredo . Hydrobiologia (submitted)

"The influence of coppper contamination on *Nereis diversicolor* bioturbation" Fernandes S, Meysman FJR, Sobral P. Marine Chemistry (submitted)

"The effect of *Nereis diversicolor* on shear strength and on the erodability of cohesive sediments under the effect of copper contamination" Fernandes S, Sobral P e Alcântara F. Journal of Sea Research (submitted)

"Clearance rates of *Cerastoderma edule* under increasing current velocity, measured in two different flumes: estimation methods and interrelation with hydrodynamics" Fernandes S, Sobral P e Van Duren L. Continental Shelf Research (submitted)

"Nereis diversicolor effect on the stability of cohesive intertidal sediments". Fernandes S, Sobral P e Costa MH. Aquatic Ecology (accepted)

Oral and Poster Presentations

"Effects of copper contamination on bioturbation and modification of sediment properties". P. Sobral and S. Figueiredo. To the 8th National Conference on the Environment CNA, Lisbon , 27-29 October 2004

"Bioturbação e modificação das propriedades do sedimento após exposição ao cobre." P. Sobral, S. Figueiredo, 9th Meeting of the Portuguese Ecological Society, Coimbra. 14-16 October 2004

"Erosion thresholds of undisturbed cohesive sediments after bioturbation by *Nereis diversicolor"*. P. Sobral and S. Figueiredo, to the ECSA Local Meeting. Lisbon 9-10 September 2004.

"The effect of copper contamination on the stability of sediments bioturbated with *Nereis diversicolor*" Fernandes S e Sobral P to the 8th International Estuarine Biogeochemistry Symposium. 16-20 May 2004. Chesapeake Biological Laboratory, Maryland, USA

"Bioturbation by *Nereis diversicolor* and stability of estuarine sediments." Fernandes S, Sobral P, to the 87th Annual Meeting of the Ecological Society of America, Tucson, Arizona.USA. 4-9 August 2002